CHALMERS
UNIVERSITY OF TECHNOLOGY

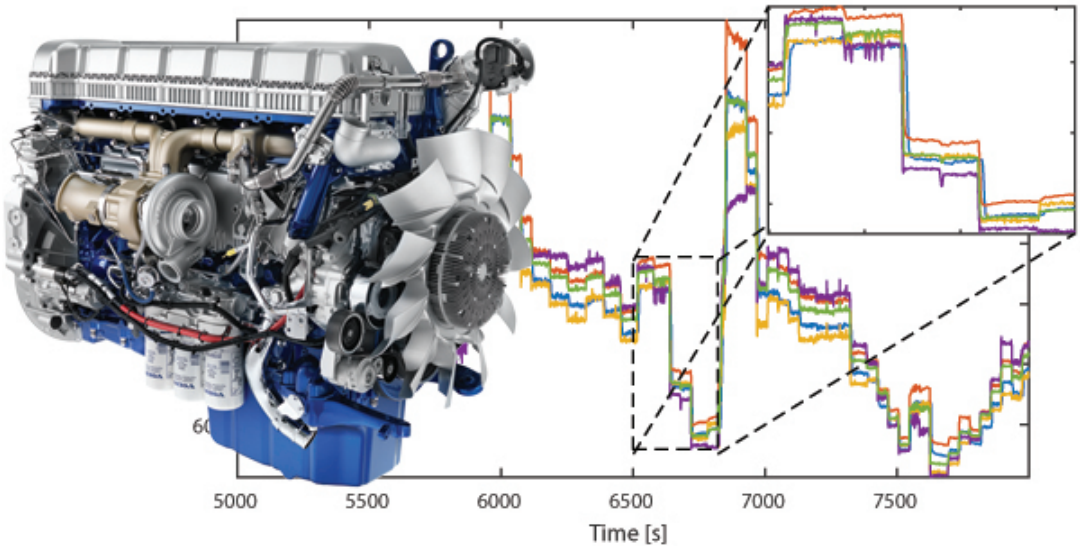

Engine out NO_x estimation in a heavy duty diesel engine

Using sensor fusion techniques to estimate NO_x emissions

Master's thesis in Systems, Control and Mechatronics

ADAM ANDERSSON
JOACIM GÖRANSSON

Department of Signals and Systems
CHALMERS UNIVERSITY OF TECHNOLOGY
Gothenburg, Sweden 2017

Master's thesis 2017:EX055

Engine out NO_x estimation in a heavy duty diesel engine

Using sensor fusion techniques to estimate NO_x emissions

ADAM ANDERSSON
JOACIM GÖRANSSON

CHALMERS
UNIVERSITY OF TECHNOLOGY

Department of Signals and Systems
Chalmers University of Technology
Gothenburg, Sweden 2017

Engine out NO_x estimation in a heavy duty diesel engine
Using sensor fusion techniques to estimate NO_x emissions

ADAM ANDERSSON
JOACIM GÖRANSSON

Supervisor: Johan Dahl, Volvo Group Trucks Technology Powertrain AB
Examiner: Jonas Fredriksson, Department of Signals and Systems

Master's Thesis 2017:EX055
Department of Signals and Systems
Chalmers University of Technology
SE-412 96 Gothenburg
Telephone +46 31 772 1000

Cover: Volvo 480hp 13l diesel engine (© Volvo Trucks) together with MATLAB© plot of NO_x emissions.

Typeset in LaTeX
Gothenburg, Sweden 2017

Engine out NO_x estimation in a heavy duty diesel engine
Using sensor fusion techniques to estimate NO_x emissions
ADAM ANDERSSON
JOACIM GÖRANSSON
Department of Signals and Systems
Chalmers University of Technology

Abstract

This thesis investigates the possibility to estimate NO_x emissions more precise than what is accomplished today by the built in NO_x sensor in a heavy duty truck from Volvo GTT. Empirically determined engine out NO_x models are compared to each other but also a physical NO_x model is developed. The developed NO_x model requires cylinder pressure and cylinder temperature as inputs, therefore models for these two variables are developed as well. The results obtained from the NO_x model are constantly underestimated but follow trends and variations in a satisfactory way. Two Kalman filters are developed, a linear Kalman filter with a constant velocity motion model and a Cubature Kalman filter that uses the developed NO_x model as motion model. Both devolped Kalman filters uses the empirical models together with a vehicle NO_x sensor as measurements. The results from the linear Kalman filter and the Cubature Kalman filter look promising, both of the filters result in better estimations than what is accomplished by the NO_x sensor used in today's vehicles. The linear Kalman filter performs a bit worse than the Cubature Kalman filter but is about 8000 times faster regarding computational speed, therefore this filter might be better to use in a real world implementation.

Keywords: CKF, KF, NO_x estimation, pressure estimation, sensor fusion, temperature estimation.

Acknowledgements

We would like to thank the EATS control team at Volvo GTT for giving us the opportunity to carry out this thesis. A special thanks goes to Jonas Fredriksson our supervisor and examiner at Chalmers and to Johan Dahl our supervisor at Volvo GTT whom have contributed to meaningful discussions throughout this thesis.

Adam Andersson, Joacim Göransson, Gothenburg, June 2017

Contents

List of Figures

List of Tables

Nomenclature

Chemical

$\Delta h^{\circ}_{f,i}$	Enthalpy of formation for species i
$[X]$	Concentration of specie X
$[X]_e$	Equilibrium concentration of specie X
$f_i(p,T)$	Mole fraction function for specie i
h_i	Molar specific enthalpy of species i
h°_i	Enthalpy of species i relative to reference state; $T_0 = 298.15$ K, $p_0 = 1$ atm
k^+_i	Forward reaction rate constant
k^-_i	Reverse reaction rate constant
K_p	Equilibrium constants
R	The gas constant
R_i	Chemical reaction

Engine parameters

αEOI	Angle at end of injection
αSOI	Angle at start of injection
δ	Injected fuel mass
θ	Crank angle degree (CAD)
$boostP$	Boost pressure
n_{eng}	Engine speed
V	Cylinder volume
W_{fuel}	Fuel mass flow
BDC	Bottom Dead Center
EATS	Exhaust After Treatment System
ECU	Electronic Control Unit
EGR	Exhaust Gas Recirculation
EOI	End of Injection
SCR	Selective Catalytic Reduction
SOI	Start of Injection
TDC	Top Dead Center

Modelling and Filtering

γ	Ratio of specific heats
C_i	Model constants
c_p	Specific heat capacity at constant pressure

h_c	Heat transfer coefficient
p	Cylinder pressure
Q	Heat release
T	Cylinder temperature
T_{burn}	Burned zone temperature
$T_{flame,ad}$	Adiabatic flame temperature
CKF	Cubature Kalman Filter
KF	Kalman Filter

1

Introduction

The four stroke diesel engine is an engine with high thermal efficiency and is often the engine of choice in trucks. The diesel engine does not have a sparkplug to ignite the fuel, as most petrol engines do, but it uses the high temperature achieved by compressing the gas causing the fuel to be ignited instead. A more detailed illustration of how the four strokes work can be seen in Figure 1.1.

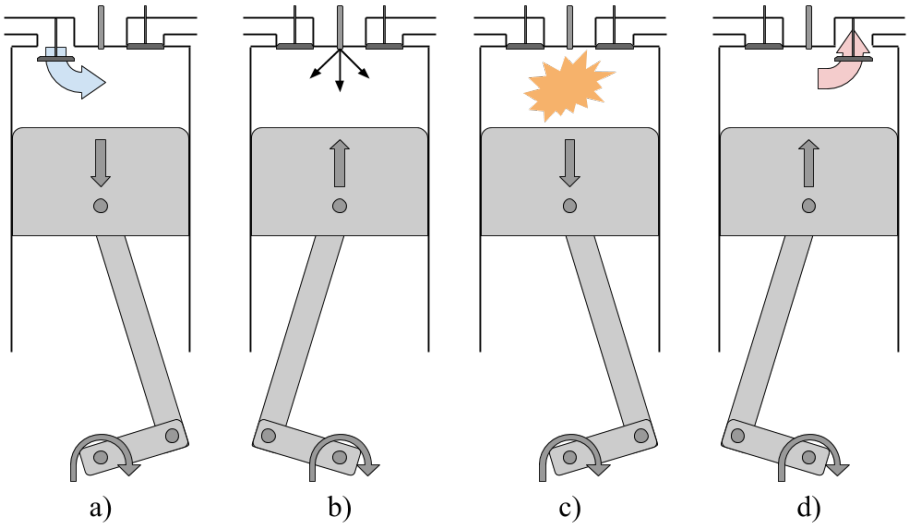

Figure 1.1: *Illustration of the engine cycle of a four stroke compression-ignition diesel engine. a) Intake, b) Compression, c) Expansion, d) Exhaust.*

a) The intake valve is open and air is sucked in to the cylinder as the piston goes down.
b) When the piston reaches Bottom Dead Center (BDC) the inlet valve is closed and the compression phase begins as the piston moves up. When the piston is close to the Top Dead Center (TDC) the injection of fuel begins.
c) Due to the high temperature caused by the compression of the gas in the cylinder the injected fuel is ignited. This causes a rapid change in pressure which forces the piston down.
d) When the piston reaches BDC the exhaust valve is opened and the exhaust gas leaves the cylinder.

It is well known that combustion of fossil fuel causes pollution due to emissions of carbon monoxides (CO), hydrocarbons (HC), particulate matter (PM), nitric oxides (NO), nitrogen dioxides (NO_2), smoke and soot, [1]. When talking about both NO

and NO_2 a popular abbreviation is NO_x. The process that produces NO_x during combustion can be divided into three mechanisms, namely; thermal, fuel and prompt NO_x, described in [2].

The thermal NO_x mechanism is the main contributor to NO_x emissions in diesel combustion. This mechanism is often referred to as the *extended Zeldovich mechanism*, [3] which can be described using equilibrium reactions:

$$O + N_2 \leftrightarrow NO + N \tag{1.1}$$

$$N + O_2 \leftrightarrow NO + O \tag{1.2}$$

$$N + OH \leftrightarrow NO + H \tag{1.3}$$

The concentration of this thermal NO_x mechanism is highly dependent on the temperature during combustion, as it requires very high temperatures (in excess of 1500 K, [2]) to form NO_x due to the strong triple bond in the N_2 molecule, [4]. The concentration of oxygen and nitrogen available during the combustion also affects to which extent thermal NO_x is created.

Fuel NO_x is formed by oxidation of the fuel bound nitrogen. The reaction from the nitrogen in the fuel to NO occurs by producing nitrogen compounds, HC_n, amines and cyanides from the pyrolysis, [4]. This mechanism is however not a major contributor of the NO_x formation in a diesel engine but more present during combustion of oil and coal, as described in [4].

Prompt NO_x or the *Fenimore mechanism* is another source of NO_x in combustion. This has been found to form promptly in the flame front, which is what it has been named after, due to reaction of nitrogen in the air with hydrocarbon radicals from the fuel. This mechanism is however considered as less important than what the thermal NO_x mechanism is at temperatures that are present for diesel combustion, according to [5].

Due to the emissions several standards have been legislated. In Europe the legislations are called Euro I - Euro VI, where Euro VI is the latest legislation introduced in January 2013 and it is also the most restricted so far. If the Euro V and the Euro VI standards are compared it is seen in Table 1.1 that it is the NO_x regulations that have been affected most significantly, [6, 7].

Table 1.1: *EU emission standards for heavy duty diesel engines in steady state testing for Euro V and Euro VI.*

Standard	CO	HC	NO_x	PM
	g/kWh			
Euro V	1.5	0.46	2.0	0.02
Euro VI	1.5	0.13	0.4	0.01

In Figure 1.2 the CO emissions and the NO_x emissions for Euro I to Euro VI are illustrated. As can be seen, the CO emissions have not been changed since Euro IV while the NO_x emissions have decreased significantly over the past years.

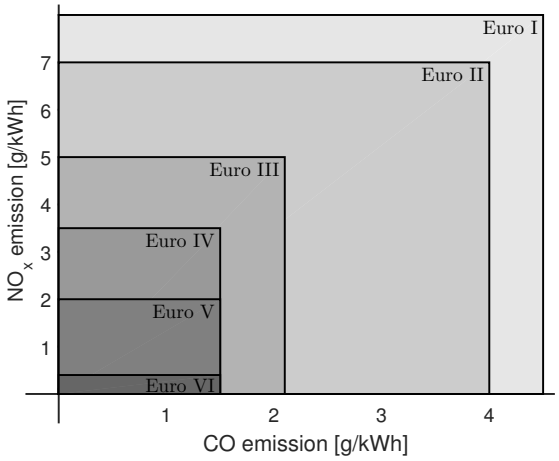

Figure 1.2: *Illustration of emission regulations of NO_x and CO for Euro I - Euro VI.*

Due to sharpened regulations the demand on control of heavy duty diesel engines have increased. For future regulations Volvo Group Trucks Technology Powertrain AB (further on called Volvo) have to be able to control the emissions further, especially the NO_x emissions. To be able to achieve this a reliable measurement or estimation method of the NO_x emissions have to be designed. A variety of NO_x models exist, such as mean valued engine models [8], zero-dimensional one-zone thermodynamical models [9], super-extended Zeldovich mechanism models [10] etc. Typically NO_x sensors are used for the control feedback but in many cases the sensor accuracy is too low and in some cases there is no available sensor data at all. To be able to meet upcoming regulations a reliable NO_x estimation method has to be available, where Volvo want to include sensor fusion techniques. Here sensor fusion means that information from several sensors and models are fused together to be able to get a result with less uncertainty than the individual sensors or models would give by using them separately.

1.1 Purpose and aims

The objective of this thesis is to use sensor fusion techniques in order to improve the estimation of NO_x formation in a heavy duty diesel engine. This is to be done with engine out NO_x models and sensor data from NO_x sensors and from other available sensors. The estimation method should be implemented, simulated and tested in MATLAB© and have real time implementation in mind regarding computational efficiency.

A set of sub problems subject to questions which need to be answered in order to reach a satisfactory result was created:

- Development and evaluation of NO_x models:
  1. Which type of NO_x model should be used?
  2. Is it possible to use multiple NO_x models simultaneously?

   3. Under which conditions do(es) the model(s) work, i.e. gives a valid estimation?
   4. Can information from different models be combined and weighted in order to get a better estimation for a larger range of conditions?
- Analysis and use of sensors:
   1. What sensors are available in the ECU and what sensors are appropriate to use?
   2. How accurate are the sensors and under which conditions do they work?
- Sensor fusion and filtering:
   1. What filtering method should be used?
   2. If multiple models are used, how are the information from these best fused together in order to get satisfactory results over a large range of working conditions?
   3. How are the information from the sensors and models combined to get an accurate estimate?
   4. Is the difference in performance between filters large enough to draw some conclusion regarding computational efficiency?

1.2 Scope and boundaries

The scope of the thesis is to estimate engine out NO_x more correct than what is accomplished today. By more correct means that the overall NO_x estimation over time is taken into consideration. Since no ground truth data is available, the most accurate NO_x sensor which is only available in an engine cell and not in the ECU in the trucks is considered as the truth instead. It is therefore the NO_x sensor in the engine cell that all the NO_x estimation results are compared to since it is considered to be closest to the truth. To be able to estimate the NO_x emissions better than what is accomplished today engine out NO_x models, the NO_x sensor, other sensors that are available in the ECU and sensor fusion is used. Since this problem is highly non linear different filter methods are evaluated with main focus on different Kalman filters and sigma point methods.

This thesis does not aim to create a new way of modelling NO_x but instead use available information to model the desired system behaviour. Experimental data will be provided by Volvo so no additional experiments will be performed during this thesis in order to affect current engine out NO_x performance. Only currently available sensors in the ECU together with sensors in the engine cell are used. The NO_x estimation will be restricted to a heavy duty diesel engine, i.e. there is no guarantee that the NO_x estimation can be applied to other engines/systems without modifications.

1.3 System overview

The data used for simulation and validation comes from a 6 cylinder, 480 hp diesel engine using Selective Catalytic Reduction (SCR). SCR is a process for reducing

the amount of NO_x emissions, this process does however occur in the Exhaust After Treatment System (EATS) and does not affect the engine out NO_x emissions, which is what is measured and estimated in this thesis. Another way of reducing the NO_x emissions is to use Exhaust Gas Recirculation (EGR), which reduces the NO_x emissions by recirculating a fraction of the exhaust gas back to the intake manifold. EGR is thus a process that affects the engine out NO_x, however this process is not used on the engine used in this thesis. In Figure 1.3 an overview of an engine is seen which includes the EGR hardware for illustration.

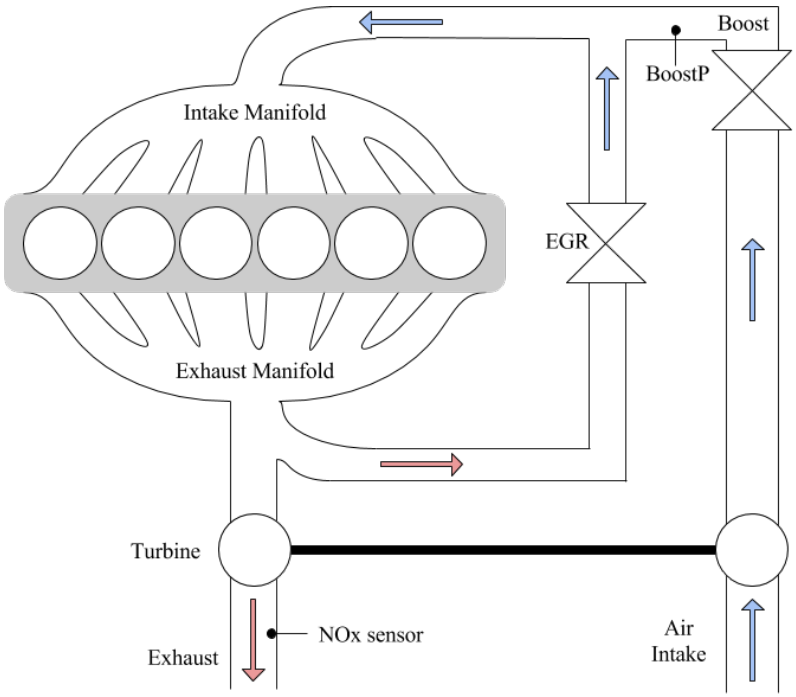

Figure 1.3: *Overview of a 6 cylinder diesel engine with EGR together with NO_x sensor and boost pressure sensor denoted $BoostP$.*

1.4 Thesis outline

This section describes the layout of the thesis. First three chapters presenting the different parts of the model are presented. First the cylinder pressure model is described followed by the cylinder temperature model and last the NO_x model is presented which uses the output from both the cylinder pressure model and the cylinder temperature model. The modelling chapters are followed by the sensor fusion chapter where both filtering theory and the filter implementation used in this thesis are presented. Finally the results, the discussions and the conclusion are presented.

2

Cylinder pressure model

To be able to model the NO_x formation also the cylinder pressure has to be available. Today there is no cylinder pressure sensor available in the ECU but only in the engine cell. Therefore the cylinder pressure has to be estimated and modelled as well. This chapter is outlined by first presenting fundamental calculations and underlying theory for cylinder pressure estimation, followed by assumptions that have been made to the model to work in practice and finally results from the cylinder pressure model are presented.

2.1 Fundamental theory and calculations to model cylinder pressure

By rearranging the first law of thermodynamics it is possible to create an expression that calculates the pressure rate with respect to crank angle θ, according to [11],

$$\frac{dp}{d\theta} = \left(\frac{dQ_n}{d\theta} - \frac{\gamma}{\gamma - 1} p \frac{dV(\theta)}{d\theta}\right)\left(\frac{\gamma - 1}{V(\theta)}\right) \tag{2.1}$$

where p is the cylinder pressure, dQ_n is the heat release rate, $V(\theta)$ is the cylinder volume, $\frac{dV(\theta)}{d\theta}$ is the rate of change in volume and $\gamma = \frac{c_p}{c_v} \approx 1.3$ is the ratio of specific heats.

2.1.1 Cylinder volume calculations

The cylinder volume is only dependent on engine geometry together with the crank angle θ and is calculated as:

$$V(\theta) = V_c + \frac{\pi B^2}{4}\left(l + a + a\cos(\theta) - \sqrt{l^2 - a^2\sin^2(\theta)}\right) \tag{2.2}$$

The rate of volume change $\frac{dV(\theta)}{d\theta}$ is the crank angle derivative of the volume and is calculated as:

$$\frac{dV(\theta)}{d\theta} = \frac{\pi a B^2}{4}\sin(\theta)\left(1 + a\cos(\theta)\left(l^2 - a^2\sin^2(\theta)\right)^{-1/2}\right) \tag{2.3}$$

The volume is completely based on engine geometry, this is illustrated in Figure 2.1 where V_c is the clearance volume, B is the cylinder bore, a is the crank radius and l is the length of the connecting rod.

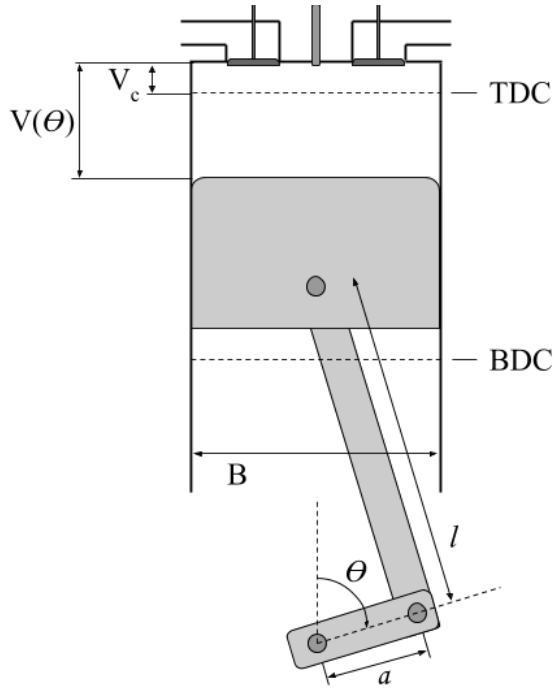

Figure 2.1: *Illustration of the engine geometry used to calculate the cylinder volume based on the crank angle θ.*

2.1.2 Heat release rate calculations

In order to calculate (2.1) the heat release rate has to be calculated. The heat release rate is substantial when the injected fuel is ignited due to compression as explained in Figure 1.1 (c). When the fuel ignites and explodes, the cylinder pressure is affected drastically and therefore it is natural to include the heat release rate for the cylinder pressure calculations. The net heat release rate is calculated according to:

$$dQ_n = dQ_g - dQ_{ht,conv} - dQ_{ht,rad} \tag{2.4}$$

where dQ_n is formed by three terms, namely the gross heat release rate dQ_g, the convective heat loss rate $dQ_{ht,conv}$ and the radiative heat loss rate $dQ_{ht,rad}$, see [11].

The gross heat release rate dQ_g is calculated as:

$$dQ_g = \begin{cases} 0 & \theta < \alpha_{SOC} \\ C_1 \left(Q_{fuel,inj} - Q_g\right) & \alpha_{SOC} \leq \theta < \alpha_{SODC} \\ C_2 \left(Q_{fuel,inj} - Q_g\right) & \alpha_{SODC} \leq \theta \end{cases} \tag{2.5}$$

where C_1 and C_2 are empirically determined constants to match the heat release rate in simulations to real engine data and $Q_{fuel,inj}$ is the injected fuel energy at a crank angle θ according to:

$$Q_{fuel,inj} = Q_{LHV} \int_{\alpha_{SOI}}^{\theta} W_{fuel}\left(\theta\right) d\theta \tag{2.6}$$

W_{fuel} is the fuel mass flow, α_{SOI} is the crank angle for the start of injection (SOI) and Q_{LHV} is the lower heating value which is approximately 42.6 MJ/kg for diesel.

It is seen that before the start of combustion (SOC) there is no heat release. In the interval from start of combustion (SOC) to start of diffusion combustion (SODC), the injected fuel during the ignition delay is added to the gross heat release calculation. The ignition delay is the period from that the fuel is injected in the cylinder to the point that the fuel is ignited. After SODC the main contribution to the gross heat release rate calculation is added since most of the combustion is performed when $\alpha_{SODC} \leq \theta$.

The convective heat losses are calculated as:

$$dQ_{ht,conv} = A(\theta)h_c\left(T - T_{wall}\right), \qquad T_{wall} = 450K \tag{2.7}$$

where $A(\theta)$ is the instantaneous surface area of the cylinder according to:

$$A(\theta) = \frac{\pi B^2}{2} + \pi Ba \cdot \left(\frac{l}{a} + 1 - \cos(\theta) + \sqrt{\left(\frac{l}{a}\right)^2 - \sin^2(\theta)}\right) \tag{2.8}$$

T is the cylinder temperature from the previous crank angle step, T_{wall} is set to a fixed value of 450 K and

$$h_c = CB^{m-1}p^m T^{0.75-1.62m} \cdot \left[C_1 v_p + C_2 \frac{V\Delta p}{V_0 p_0} T_0\right]^m \tag{2.9}$$

is the heat transfer coefficient determined by Woschni in [12].

The constants $C = 3.26$, $C_1 = 2.28$ and C_2 in the heat transfer coefficient are determined by Woschni. C_2 is set to different values depending on where in the combustion cycle the process are, i.e. compression or expansion. In case of compression $C_2 = 0$ and in the expansion case $C_2 = 3.24 \cdot 10^{-3}$. The exponent term $m = 0.8$ is selected empirically, B is the cylinder bore, v_p is the mean piston speed, Δp is the instantaneous pressure difference in cylinder and motor pressure. V_0, T_0 and p_0 is the reference volume, temperature and pressure at a certain point in the combustion process respectively, for example at intake valve close (IVC).

The radiative heat losses are

$$dQ_{ht,rad} = C_{rad}\left(n_{eng}, \delta\right) T_{flame}^4 \tag{2.10}$$

where

$$C_{rad}\left(n_{eng}, \delta\right) = c_0 + c_1 \cdot n_{eng} + c_2 \cdot \delta \tag{2.11}$$

C_{rad} is a semi-empirically determined expression used to fit the simulated model to measurements where n_{eng} is the engine speed, δ is the injected fuel mass and T_{flame} is the flame temperature calculated as in Section 3.1.

2.2 Assumptions for cylinder pressure model

From the theory of calculating the cylinder pressure some simplifications has been made to the cylinder pressure model. These simplifications have been made in order to reduce the computational effort of the model but still get a satisfactory result. The pressure model uses two intervals defined by the start of combustion (αSOC) in (2.5). The αSOC occurs some time after the fuel injection has started and this time differs between cycles but has in the model been set to a fixed value. When the model was tested and tuned it was clear that the convective heat losses $dQ_{ht,conv}$ did not contribute a lot to the final result. Therefore $dQ_{ht,conv}$ was excluded in the implementation of the pressure model. The following subsections will go further into details about other assumptions and simplifications made.

2.2.1 Choice of initial pressure

To be able to calculate the cylinder pressure as in (2.1) it is necessary to know the cylinder pressure from the previous crank angle step. This is performed iterative during the process, however initially the cylinder pressure value has to be determined. In this section an investigation of how to determine this value and what impact it has to the final cylinder pressure result is presented. The starting value of the pressure estimation is of high importance to the result of the cylinder pressure estimation. In Figure 2.2 the area where the starting pressure value should be chosen is highlighted.

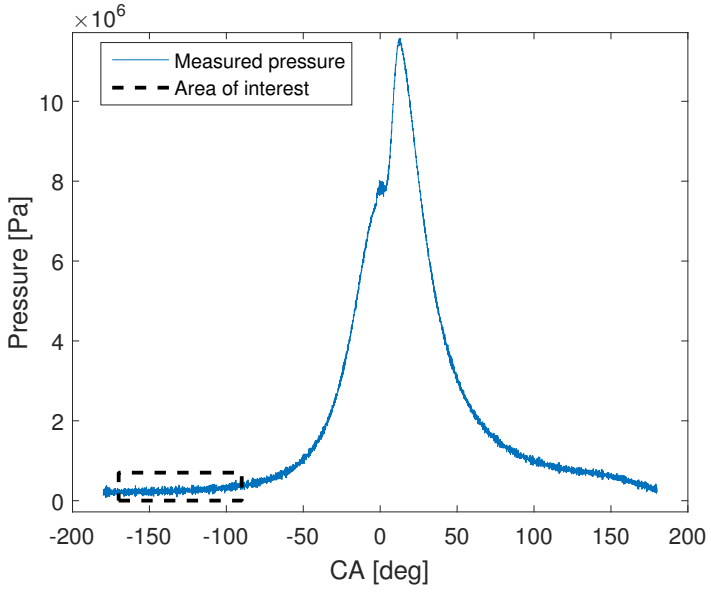

Figure 2.2: *Highlighted area of interest where the initial pressure should be determined.*

As can be seen in Figure 2.3 a small change in the initial pressure value has a large impact of the behaviour of the resulting cylinder pressure curve. To the left the

initial pressure is set to 0.22 MPa while the resulting cylinder pressure curve to the right has an initial pressure set to 0.26 MPa.
As seen the pressure curves are affected significantly by the small variation in the initial pressure. Since the temperature estimation is dependent of the pressure estimation it is necessary to be able to estimate the initial pressure well, if this can not be done well enough also the NO_x estimation will suffer and the overall result becomes less accurate.

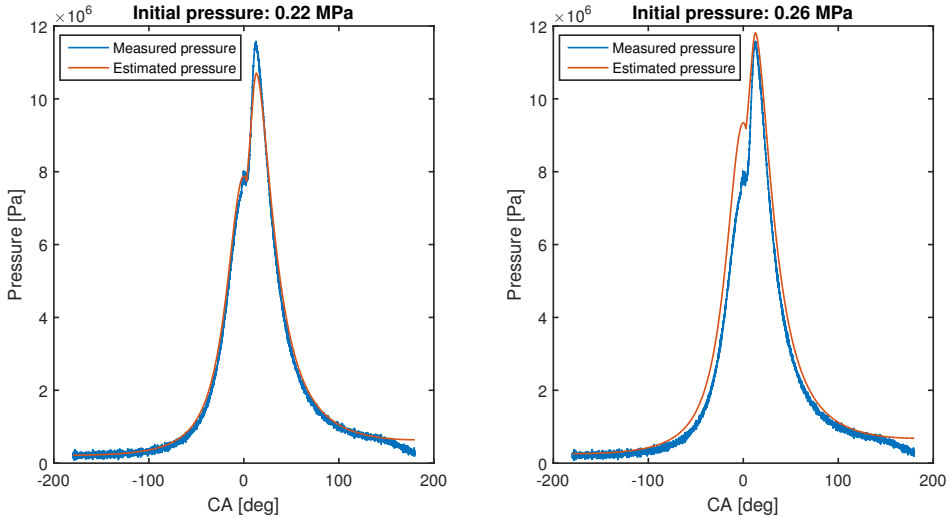

Figure 2.3: *Illustration of impact for resulting cylinder pressure curves due to small changes in initial pressure. Left: Initial pressure set to 0.22 MPa. Right: Initial pressure set to 0.26 MPa.*

To be able to model the cylinder pressure correctly a measure for the initial pressure has to be used. In Figure 2.4 the cylinder pressure in the highlighted area shown in Figure 2.2 have been selected and the mean values and the variances have been calculated and are illustrated in form of error bars for different engine speeds. This is compared to the boost pressure that is available in the ECU and some similarities are found, at least the curves seem to have a similar trend. Even though the two curves do not match exactly this was the best measure that was found available in the ECU, therefore the boost pressure was selected to be used as the initial pressure for the pressure model.

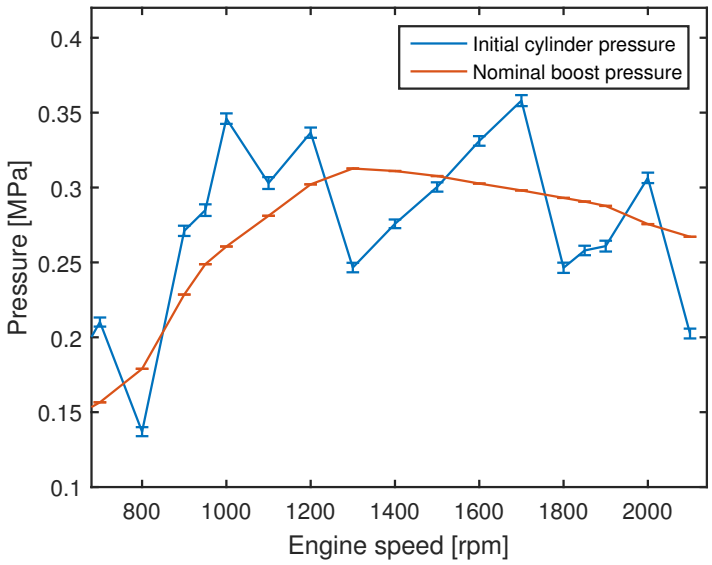

Figure 2.4: *Comparison of initial cylinder pressure and boost pressure with mean values and variances shown as error bars.*

2.2.2 Fuel injection behaviour

The injection of fuel into the cylinder is performed between the angle of start of injection (αSOI) and end of injection (αEOI). The behaviour of the fuel flow in this interval is not a trivial thing to model so a simplification has been made for the injected fuel. It is assumed that there is no delay in the injector needle which results in a very fast and exact injection. The assumed fuel injection has been illustrated in Figure 2.5 where the area under the curve corresponds to the total amount of injected fuel for one combustion cycle.

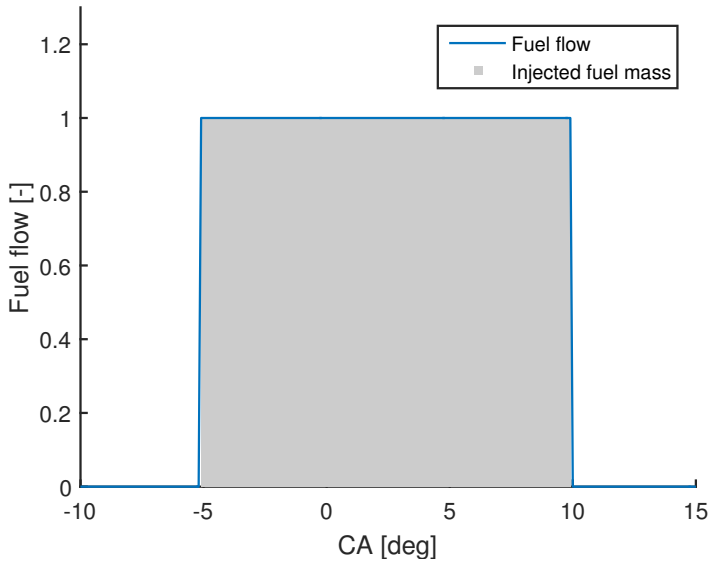

Figure 2.5: *Illustration of the fuel injection behaviour.*

For this illustration the αSOI is set to -5 CAD and αEOI to 10 CAD. The magnitude of the graph does not correspond to any real values of the fuel flow but is only used for illustrative purpose.

2.3 Cylinder pressure results

Since no cylinder pressure sensor is available in the ECU, measurements from the engine cell have been used to validate the cylinder pressure model. In Figure 2.6 six different cylinder pressure results are shown, the results are performed for different engine speeds at full load. As can be seen, the estimated cylinder pressure corresponds to the measured cylinder pressure in a satisfactory way for most of the cases. It is seen that when 700 rpm and 2100 rpm are used the estimated cylinder pressure differs the most, however those engine speeds are at the extremes of the range and it is more important that the model estimates the cylinder pressure correct for engine speeds that are used during normal working conditions.

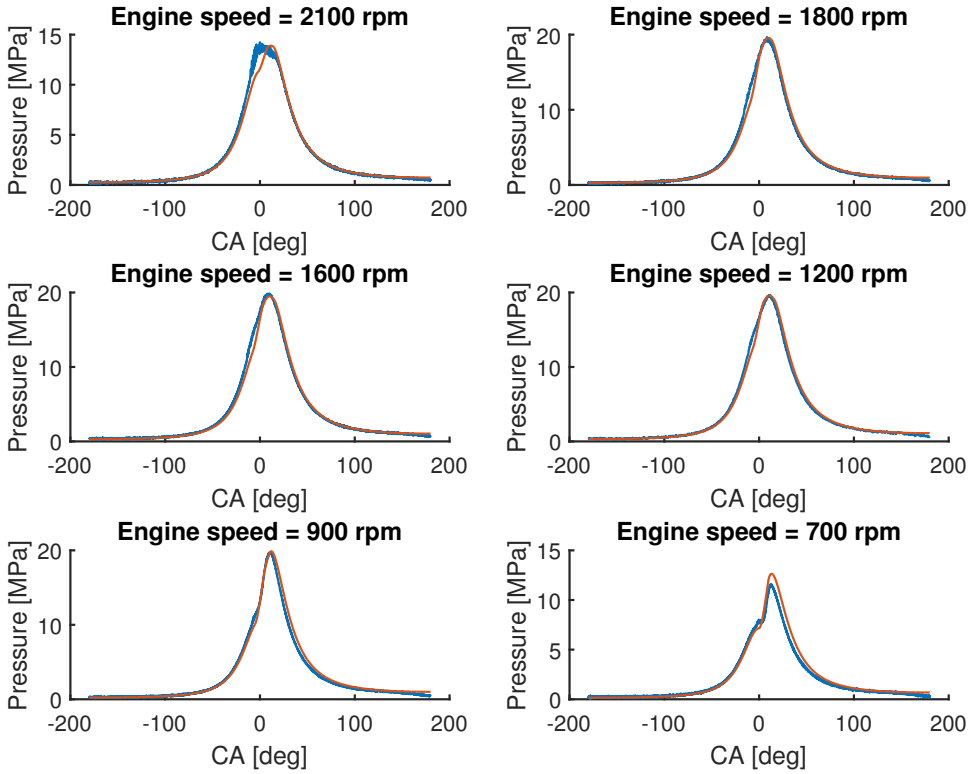

Figure 2.6: *Comparison between measured cylinder pressure (blue curve) and estimated cylinder pressure (red curve) at different engine speeds.*

One measure to quantify how the model performs is to compare the maximum cylinder pressure. In Figure 2.7 a comparison of maximum cylinder pressure during the combustion cycle is shown for different engine speeds together with the absolute

error between the measurement and the estimation from the model. Using a measure like this does not say anything about how well the curves correspond to each other more than just the peak value but this is on the contrary already shown in Figure 2.6. As can be seen the maximum absolute error is about 1 MPa which will affect the cylinder temperature and the NO_x calculations but it is still considered as a satisfactory result.

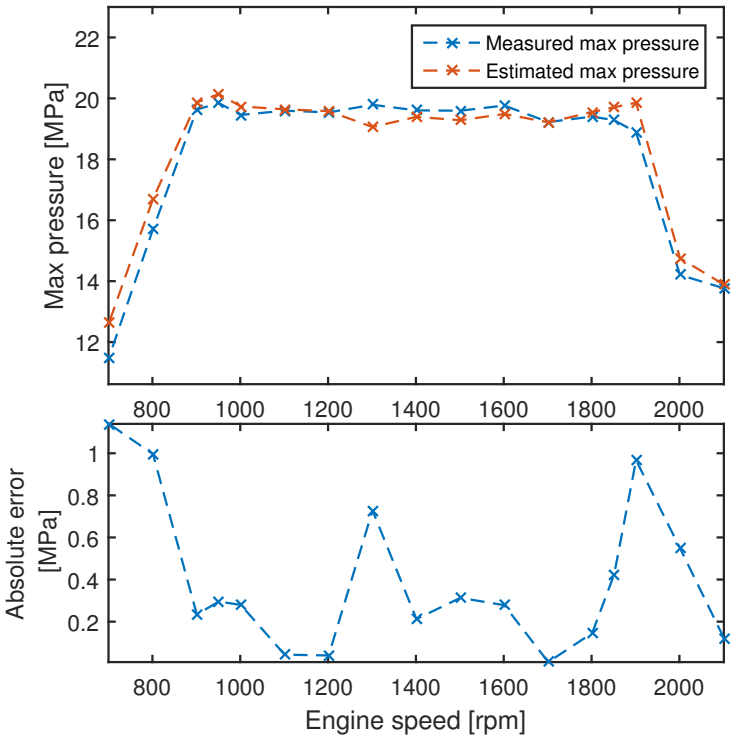

Figure 2.7: *Comparison of estimated and measured maximum cylinder pressure and absolute error for different engine speeds.*

In Figure 2.8 a steady state simulation for maximum cylinder pressure is shown, overall the estimated cylinder pressure corresponds to the measured cylinder pressure. The absolute error are larger for some areas but it is also relatively small for most of the simulation. Since the result is obtained from a simulation where several different physical areas are excited, the simulation is a good measure to see how dynamic the model is. Even though the simulation excites so many different areas the model is still able to estimate the cylinder pressure in a satisfactory way.

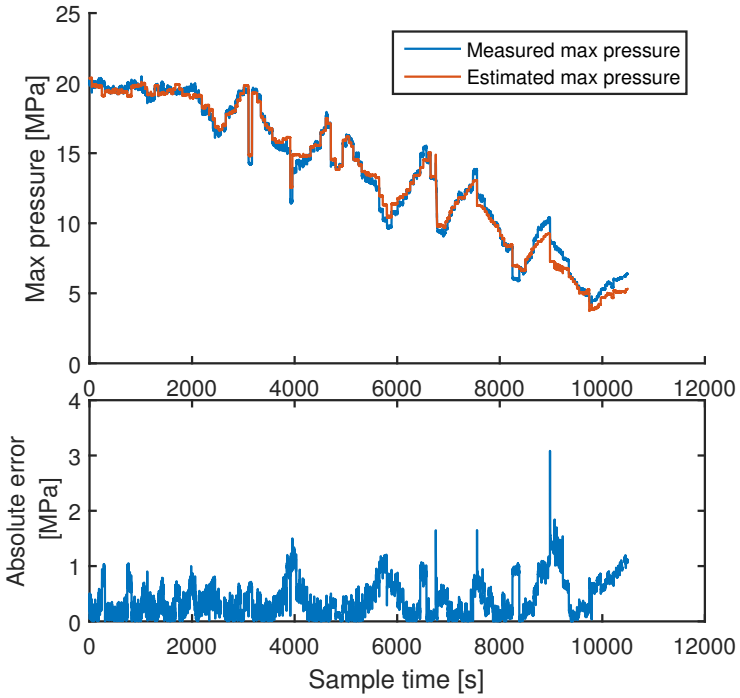

Figure 2.8: *Comparison of estimated and measured maximum cylinder pressure and absolute error at steady state simulation.*

3

Cylinder temperature model

For the cylinder pressure the cylinder temperature is required in order to model the NO_x formation. As for cylinder pressure there is no cylinder temperature sensor available in the ECU, but this time it is not available in the engine cell either. This chapter is outlined by first presenting fundamental calculations and underlying theory for cylinder temperature estimation, followed by a walk-through of how the cylinder temperature is estimated and finally results from the cylinder temperature model are presented.

3.1 Fundamental theory and calculations to model cylinder temperature

When estimating the cylinder temperature during combustion the flame temperature has to be calculated. This is done by first calculating the adiabatic flame temperature which is explained in Section 3.1.1. This adiabatic flame temperature, $T_{flame,ad}$, is then compensated for dissociation (Section 3.1.2). Dissociation is needed for temperatures over 1250 K according to [13], then the flame temperature T_{flame} can be calculated, as in [11], with

$$T_{flame} = T_{flame,ad} - f_{eq}(p, T_{flame,ad}, \lambda_{local}). \tag{3.1}$$

Here the function $f_{eq}(p, T_{flame,ad}, \lambda_{local})$ is the dissociation compensation. The radiative heat losses that occur in the combustion process are compensated for as in

$$T_{flame,ht} = T_{flame,ad} - \frac{dQ_{ht,rad}}{c_p} \tag{3.2}$$

where $dQ_{ht,rad}$ represents the radiative heat losses, depending on T_{flame}, and is explained in (2.10). Based on this temperature the burned zone temperature is calculated by using isentropic expansion/compression using

$$T_{exp} = T_{burn,perf}\left(\theta - 1\right)\left(\frac{p\left(\theta\right)}{p\left(\theta - 1\right)}\right)^{\frac{\gamma-1}{\gamma}} \tag{3.3}$$

$$T_{burn,perf}\left(\theta\right) = \frac{T_{exp}m_{burn}\left(\theta\right) + T_{flame,ht}\left(m_{burn}\left(\theta\right) - m_{burn}\left(\theta - 1\right)\right)}{m_{burn}\left(\theta\right)} \tag{3.4}$$

$$T_{burn} = T_{burn,perf}\left(\theta\right) - f_{eq}\left(p, T_{flame,ad}, \lambda_{local}\right) \tag{3.5}$$

where m_{burn} is the burnt mass, θ is the notion for current crank angle, $\theta - 1$ is the notion for previous crank angle and T_{burn} is the estimated cylinder temperature.

3.1.1 Adiabatic flame temperature calculations

The adiabatic flame temperature in combustion is the result of a complete combustion process where no heat is transferred and no work is performed. Since the combustion process in a diesel engine takes place in a very short time interval little heat is transferred and therefore the highest achieved temperature is often near the adiabatic temperature, as can be seen in [13].

For a known chemical process the adiabatic flame temperature can be calculated, for example for a fuel-lean combustion with diesel the stoichiometry is calculated with

$$CH_n + \frac{\alpha_s}{\phi}\left(O_2 + 3.78N_2\right) \rightarrow CO_2 + \frac{n}{2}H_2O + \alpha_s\left(\frac{1}{\phi} - 1\right)O_2 + \frac{3.78\alpha_s}{\phi}N_2 \tag{3.6}$$

where $\alpha_s = 1 + n/4$ and the equivalence ratio ϕ, is the fuel to air ratio normalized to the stoichiometric fuel to air ratio. By using the enthalpy of the compounds ($h_i^\circ(T) = h_i(T) - h_i(T_0) + \Delta h_{f,i}^\circ(T)$) and the first law of thermodynamics, which states that the change in the total energy of a closed system is equal to the heat supplied to the system minus the work done by the system [13], the following equation is obtained

$$\begin{aligned} h_{CO_2}^\circ(T) + \frac{n}{2}h_{H_2O}^\circ(T) + \left(O_2 + 3.78N_2\right)h_{O_2}^\circ(T) + \frac{3.78\alpha_s}{\phi}h_{N_2}^\circ(T) \\ - h_{CH_n}^\circ(T_0) - \frac{\alpha_s}{\phi}h_{O_2}^\circ(T_0) - \frac{3.78\alpha_s}{\phi}h_{N_2}^\circ(T_0) = Q - W_x = 0. \end{aligned} \tag{3.7}$$

The adiabatic flame temperature ($T_{flame,ad}$), which solves (3.7), can then be found by a numerical method.

3.1.2 Dissociation calculations

Dissociation is the process when species that are stable at ambient temperatures separate or split into smaller particles, which happens at high temperatures and high pressures. Reactions subject to dissociation are described by

$$\begin{aligned} CO + H_2O &\overset{1}{\longleftrightarrow} CO_2 + H_2 \\ H_2O &\overset{2}{\longleftrightarrow} H_2 + \frac{1}{2}O_2. \end{aligned} \tag{3.8}$$

If (3.6) is used as an example with $n = 1.8$, $\phi = 1$ and allowing incomplete combustion, the chemical equation

$$\begin{aligned} CH_{1.8} + 1.45O_2 + 5.48N_2 \rightarrow (1-x)CO_2 + xCO + (0.9-y)H_2O \\ + yH_2 + \left(\frac{x}{2} + \frac{y}{2}\right)O_2 + 5.48N_2 \end{aligned} \tag{3.9}$$

is obtained. This equation is used in order to solve the gas composition of combustion products. In order to get a first approximation of the composition, chemical equilibrium can be calculated. This assumes that sufficiently long time has elapsed for the system to be in equilibrium, which may not be the case but is however used as a first approximation.

In order to calculate the composition (3.9) has to be solved for x and y, therefore two linearly independent equilibrium equations are used. These two equilibrium equations can be used from (3.8) and are written as:

$$\begin{aligned} K_{p_1} &= \frac{1-x}{x} \cdot \frac{y}{0.9-y} \\ p^{-1/2} K_{p_2} &= \frac{y}{0.9-y} \left(\frac{x/2 + y/2}{7.381 + x/2 + y/2} \right)^{1/2} \end{aligned} \tag{3.10}$$

where K_{p_1} and K_{p_2} are the equilibrium constants for the two reactions. With these two equations x and y can be solved yielding the composition of the combustion products. With the products known a new temperature estimate can be calculated in the same way as for the adiabatic flame temperature seen in section 3.1.1. This then becomes an iterative calculation where new compositions are calculated for the new temperatures until desired precision is achieved.

3.2 Cylinder temperature estimation

As described in Section 3.1 the flame temperature can be estimated by first calculating the adiabatic flame temperature. The adiabatic flame temperature is calculated for a stoichiometric combustion of diesel ($\phi = 1$), which can be described with the chemical equation

$$CH_n + \alpha_s \left(O_2 + 3.78 N_2\right) \rightarrow CO_2 + \frac{n}{2} H_2O + \alpha_s 3.78 N_2 \tag{3.11}$$

where $\alpha_s = 1 + n/4$ and $n = 1.886$ lead to

$$CH_{1.886} + 1.4715 O_2 + 5.5623 N_2 \rightarrow CO_2 + 0.9430 H_2O + 5.5623 N_2. \tag{3.12}$$

From (3.7) an expression for the enthalpy of the compounds, can be rearranged to

$$\begin{aligned} \left[h(T) - h(T_0)\right]_{CO2} &+ 0.9430 \left[h(T) - h(T_0)\right]_{H_2O} \\ &+ 5.5623 \left[h(T) - h(T_0)\right]_{N_2} + \Delta h_{cL}(T_0) = 0 \end{aligned} \tag{3.13}$$

where $\Delta h_{cL}(T_0)$ is the mole-based enthalpy of combustion for the fuel shown in

$$\Delta h_{cL}(T_0) = -\text{LHV}\left(M_H + 1.8 M_C\right) + 0.9430\text{LHV}. \tag{3.14}$$

$\Delta h_{cL}(T_0)$ can be calculated since the lower heating value of the fuel (LHV ≈ 42.6 $^{\text{MJ}}/_{\text{kg}}$) and the molar mass of the combustion molecules M_H and M_C are known, as

described in [13].

By using data for $[h(T) - h(T_0)]_i$ taken from JANAF tables [14] and the enthalpy from (3.14) it can be solved for which temperature (3.13) holds. The tabled data used is only for a certain amount of temperatures so interpolation is needed in order to get a better temperature estimate. This is performed by finding the first temperature for which (3.13) is positive and then interpolate linearly between this temperature and the last temperature for when the equation was negative. The interpolation gives the estimation of the adiabatic flame temperature $T_{flame,ad} \approx 2260$ K. The data taken from the JANAF tables are for the pressure $p_0 = 1$ atm $= 0.1$ MPa.

Since the adiabatic flame temperature is above 1250 K compensation for dissociation is required as explained in section 3.1.2, which leads to the equilibrium relations

$$\begin{aligned} K_{p_1} &= \frac{1-x}{x} \cdot \frac{y}{0.9430-y} \\ p^{-1/2} K_{p_2} &= \frac{y}{0.9430-y} \left(\frac{x/2 + y/2}{7.5053 + x/2 + y/2} \right)^{1/2}. \end{aligned} \tag{3.15}$$

The equations shown in (3.15) can be rearranged in order to be used as nonlinear equations for solving x and y as

$$\begin{aligned} f(x,y) &= \frac{1-x}{x} \cdot \frac{y}{0.9430-y} - K_{p_1} = 0 \\ g(x,y) &= \frac{y}{0.9430-y} \left(\frac{x/2 + y/2}{7.5053 + x/2 + y/2} \right)^{1/2} - p^{-1/2} K_{p_2} = 0. \end{aligned} \tag{3.16}$$

The values for the equilibrium constants K_{p_1} and K_{p_2} can be found in JANAF tables [14] and are dependent on the temperature, which initially is set to the adiabatic flame temperature. The equations in (3.16) are solved using the `fsolve` solver in MATLAB © using starting values $x = 0.01$ and $y = 0.01$. The result after a maximum of 30 iterations can be seen in Table 3.1.

Table 3.1: *Table of result after solving nonlinear equations for dissociation.*

x	0.1107
y	0.0206
K_{p_1}	0.1795
K_{p_2}	0.0021

From these values a new temperature can be calculated similar to the method in section 3.1.1 which is the flame temperature compensated for dissociation. The compensation is in this case however small so the new flame temperature is $T_{flame} = 2256$ K.

In order to get a temperature trace during the combustion cycle, (3.3) is used. By setting the temperature to T_{flame} at start of combustion and using the cylinder pressure to create the trace, the resulting cylinder temperature trace can be seen in Figure 3.1.

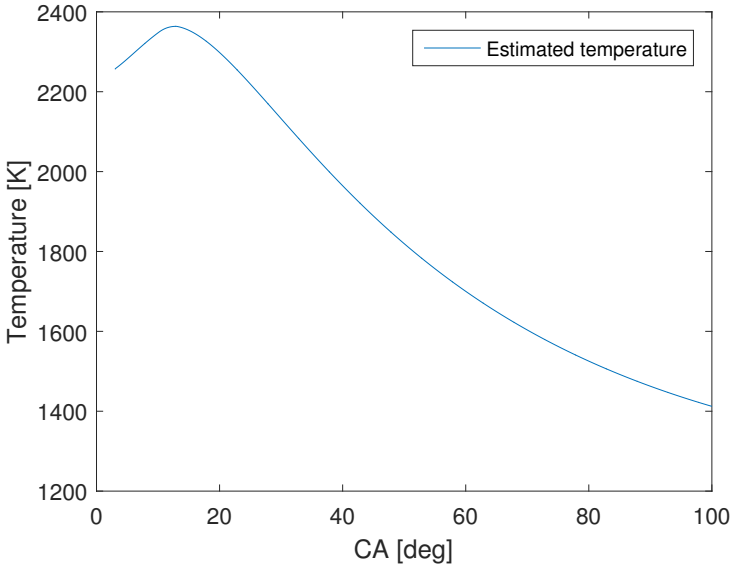

Figure 3.1: *Estimated cylinder temperature trace for one combustion cycle, starting with T_{flame} at SOC and engine speed 700 rpm.*

3.3 Cylinder temperature results

Unlike for the cylinder pressure results where a sensor is available in the engine cell, the cylinder temperature has to be completely estimated since there is no sensor measuring the cylinder temperature available. An attempt to retrieve data for comparison was performed with a simulation tool used at Volvo called GT Power, see [15]. This comparison did however not contribute as validation since the output from the simulation tool was a mean temperature and could not be directly compared to the model output which is estimated closer to the flame. In Figure 3.2 the estimated cylinder temperatures are shown for different engine speeds, note that the corresponding legend displays the peak temperature. The different cylinder temperature curves look similar to each other, however the peak values differ more than 100 K and that difference is sufficient to affect the NO_x estimation significantly.

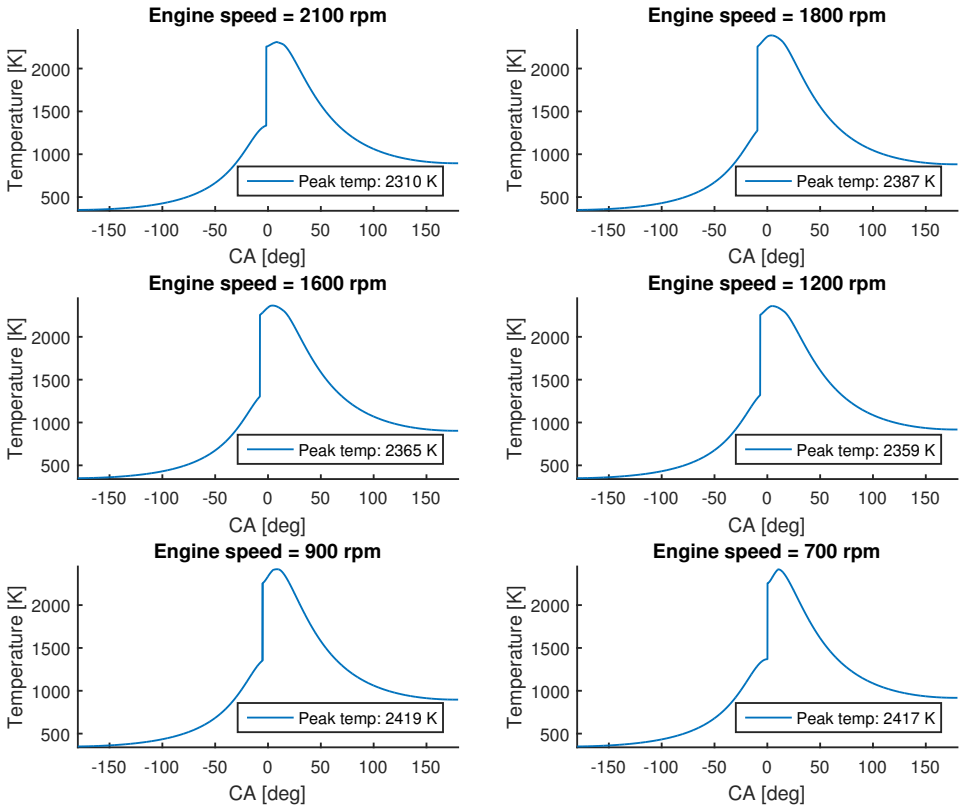

Figure 3.2: *Estimated cylinder temperature at different engine speeds, legend displays peak temperature.*

4

NO_x model

Based on the output from the cylinder pressure estimation together with the output from the cylinder temperature estimation it is possible to estimate the NO_x formation, or more correctly the NO formation which is approximately 95% of the total NO_x formation. This chapter presents the *Zeldovich mechanism*, explained in [3] which is used for the NO_x estimation, followed by a section describing how the equilibrium concentrations of species are evolving during combustion and finally estimated NO_x results from the model are presented.

4.1 The Zeldovich mechanism

As mentioned in Chapter 1 there are some chemical reactions that contribute significantly to the NO_x formation. Here the first two reactions have been taken into account, hence the *Zeldovich mechanism*;

$$\frac{d[NO]}{dt} = \frac{2R_1\left(1 - ([NO]/[NO]_e)^2\right)}{1 + ([NO]/[NO]_e)\,R_1/R_2} \tag{4.1}$$

is implemented rather than the *extended Zeldovich mechanism* described in Chapter 1. $[X]$ denotes the concentration of specie X and $[X]_e$ represents the concentration of specie X in equilibrium. R_1 and R_2 are chemical reactions according to:

$$R_1 = k_1^+[O]_e[N_2]_e, \qquad k_1^+ = 7.6 \cdot 10^{13} e^{\frac{-38000}{T}} \tag{4.2}$$

$$R_2 = k_2^-[NO]_e[O]_e, \qquad k_2^- = 1.5 \cdot 10^9 T e^{\frac{-19500}{T}} \tag{4.3}$$

where k_1^+ represents the forward reaction rate constant and k_2^- represents the reverse reaction rate constant and are determined according to Heywood in [16]. The concentration of oxygen at equilibrium

$$[O]_e = \frac{K_{p,O}[O_2]_e^{1/2}}{(RT)^{1/2}}, \qquad K_{p,O} = 3.6 \cdot 10^3 e^{\frac{-31000}{T}} \tag{4.4}$$

and the concentration of nitric oxide at equilibrium

$$[NO]_e = \left(K_{p,NO}[O_2]_e[N_2]_e\right)^{1/2}, \qquad K_{p,NO} = 20.3 e^{\frac{-21650}{T}} \tag{4.5}$$

are completely based on the temperature T, the concentration of nitrogen at equilibrium $[N_2]_e$ and the concentration of dioxygen at equilibrium $[O_2]_e$.

The concentration of nitrogen at equilibrium $[N_2]_e$ and the concentration of dioxygen at equilibrium $[O_2]_e$ are calculated using tabulated values stored in the JANAF database. The concentrations are calculated according to

$$[N_2]_e = f_{N_2}(p, T) \tag{4.6}$$

$$[O_2]_e = f_{O_2}(p, T) \tag{4.7}$$

where $f_{N_2}(p, T)$ and $f_{O_2}(p, T)$ are functions that interpolate in the matrices created in Section 4.1.1. These matrices are based on the input cylinder pressure and input cylinder temperature calculated in Chapter 2 and Chapter 3 respectively. The functions return the mole fraction for respective specie given the cylinder pressure and the cylinder temperature and are then immediately converted to concentrations.

4.1.1 Equilibrium concentrations

The equilibrium concentrations $[N_2]_e$ and $[O_2]_e$ used in the NO_x model are calculated using the same equations as for the dissociation calculations in Section 3.1.2. The linearly independent equations are solved for a range of pressure and temperature values. The result from solving the equations are stored in order to be used by the *Zeldovich mechanism* in (4.6) and (4.7). Since the results are stored for a certain range and resolution the data has to be interpolated in order to retrieve the equilibrium concentration for desired pressure and temperature.
The mole fraction can be seen in Figure 4.1 where 4.1a is the estimated mole fraction and 4.1b is taken from [13] as a comparison and validation of the result.

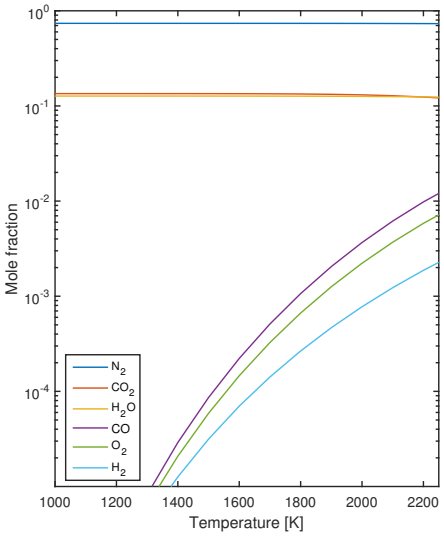

(a) *Estimated mole fraction for different temperatures at pressure $p_0 = 1$ atm. Species are ordered in legend from highest to lowest fraction.*

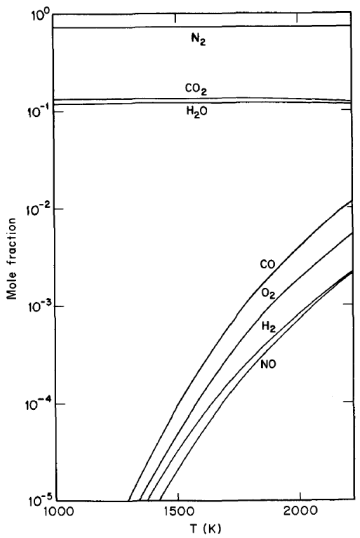

(b) *Mole fraction for different temperatures taken from [13], for comparison.*

Figure 4.1: *Comparison of mole fractions at pressure $p_0 = 1$ atm.*

For temperatures below 1300 K it can be seen that only the most stable species are present, that is N_2, CO_2 and H_2O. This corresponds well to the equations and assumptions used for calculating dissociation in Section 3.1.2, which is that for higher temperatures the stable species suffer from dissociation and the amount of the more unstable species increases.

It is important to be able to model the mole fractions of the different species to be able to estimate the NO_x formation when the engine uses EGR. However the engine that is used in this thesis does not use EGR and therefore a simplification of the model can be applied by simply setting the mole fraction for N_2 and O_2 to constant values. This model uses $0.7 \cdot N_2$ and $0.1 \cdot O_2$ which is obtained when calculating the mole fractions as before. The simplification is a reasonable assumption since there is only an intake of fresh air and no recirculation of gases which otherwise would affect the compound. Therefore the result of 70% N_2 and 10% O_2 is reasonable since the atmosphere contains about 78% N_2 and 20% O_2. Even though this simplification is done for the engine used in this thesis the model is prepared for engines that do use EGR, then the mole fraction calculations just need to be activated.

4.2 NO_x results

In Figure 4.2 different NO_x estimations are shown for different engine speeds. As can be seen is that the model behaves as it should in terms of where the NO_x formation starts and ends. For each engine speed the NO_x formation starts after the start of injection angle, αSOI and ramps up a bit further than the end of injection angle αEOI. This behaviour is natural since no NO_x can be created before any fuel is injected and it is also natural that some NO_x are created after the end of injection since that fuel has to be combusted as well.

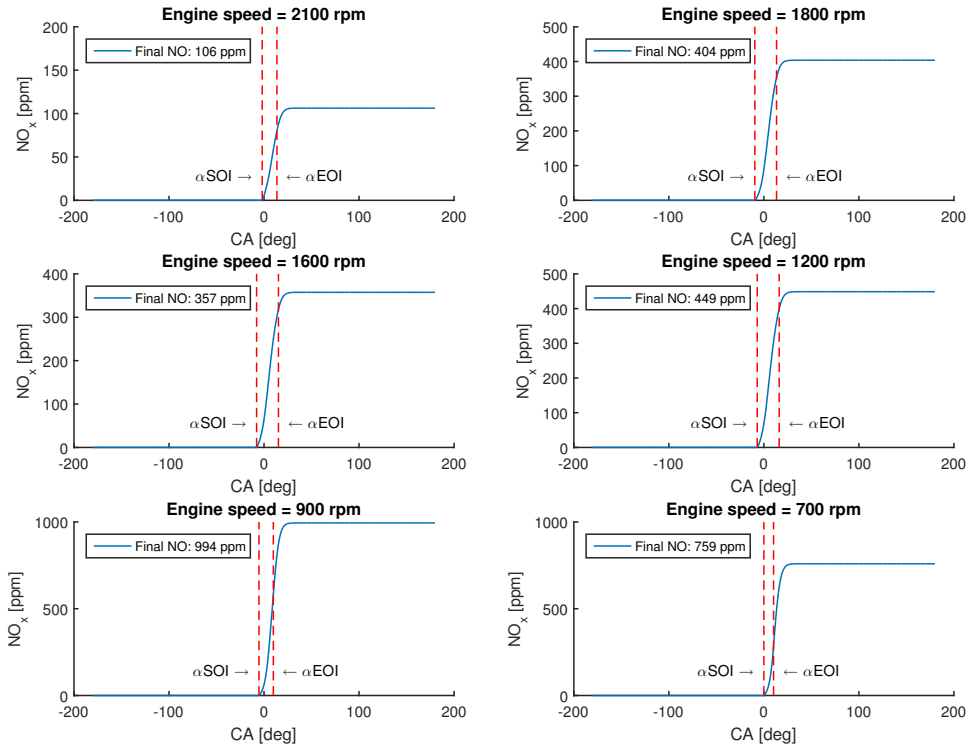

Figure 4.2: *NO_x results obtained from model at different engine speeds, note that αSOI, αEOI and the final NO_x levels are displayed.*

In Figure 4.3 and Figure 4.4 the NO_x model has been validated and compared to the NO_x sensor in the engine cell during both steady state and transient setups. As can be seen here is that the model constantly underestimates the NO_x concentration but seems to follow the trends and changes in the NO_x concentration.

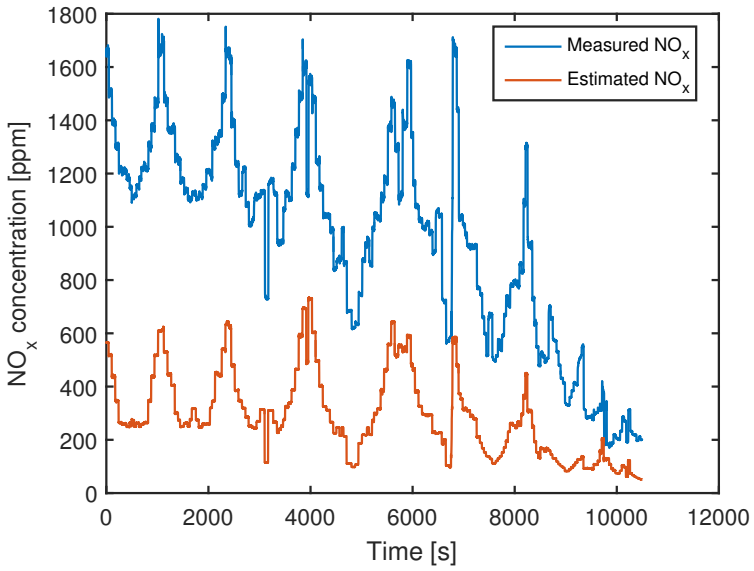

Figure 4.3: *Comparison of measured NO_x concentration and estimated NO_x concentration of a data set with a range of steady state operating points.*

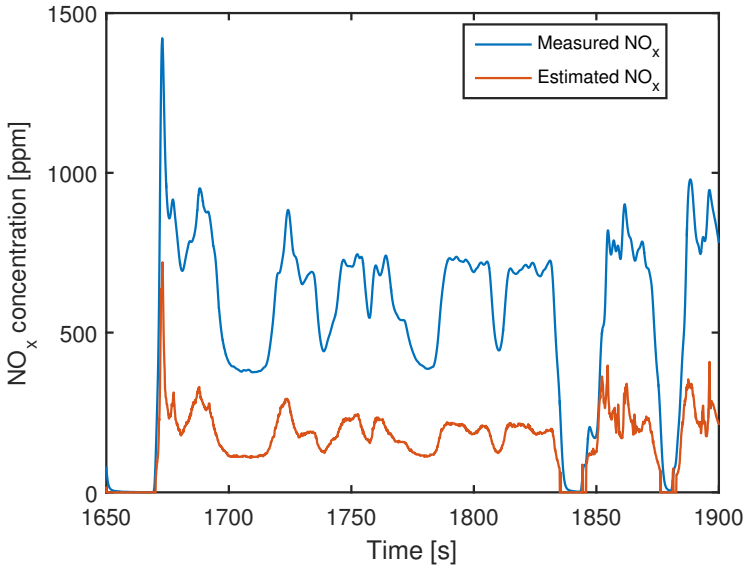

Figure 4.4: *Comparison of measured NO_x concentration and estimated NO_x concentration of a transient data set.*

5
Sensor Fusion

This chapter presents some background information of filtering but is especially concentrated at Bayesian filtering [17] together with the linear Kalman filter and the Cubature Kalman filter which is a sigma point method. Lastly the implementation of the two Kalman filters are presented, the linear Kalman filter is using a constant velocity model while the Cubature Kalman filter is using the developed NO_x model as motion model.

The reason why a linear Kalman filter with a constant velocity motion model is developed is to have a computationally cheap filter to benchmark the CKF against. To be able to use the developed NO_x model a filter that can handle nonlinearities has to be used, therefore the linear Kalman filter cannot be combined with the NO_x model. It exists several different methods for nonlinear problems such as the extended Kalman filter (EKF), the unscented Kalman filter (UKF) , the Cubature Kalman filter etc. The reason that the Cubature Kalman filter is developed is that it contains no tuning parameters and it does not require linearization as the EKF does.

5.1 Bayesian Filtering

The purpose of Bayesian filtering, based on Bayesian statistics is to recursively calculate the posterior distribution. The posterior distribution is the distribution of interest and is represented as:

$$p(\mathbf{x}_k|\mathbf{y}_{1:k}) \tag{5.1}$$

$\mathbf{x}_k$ is the state at the discrete time instant k given the observed measurement history $\mathbf{y}_{1:k}$ from time instant 1 to k, where $\mathbf{y}_{1:k} = \{\mathbf{y}_1, \mathbf{y}_2, ..., \mathbf{y}_k\}$ is a set of observed measurements collected by one or several sensors. As can be seen the distribution is a conditional probability and therefor Bayes' rule can be applied as

$$p(A|B) = \frac{p(B|A)p(A)}{p(B)} \tag{5.2}$$

where A and B are events, $p(B) \neq 0$, $p(A)$ and $p(B)$ are the probabilities that the events occur independently of each other. Hence $p(A|B)$ is the conditional probability to observe event A given that event B is true.

Another assumption that is commonly used in Bayesian statistics and filtering is

the Markov property. Here the Markov property means that the state at time k; $\mathbf{x}_k$ is only conditionally dependent on the preceding state at time $k-1$; $\mathbf{x}_{k-1}$. Also a measurement at time k; $\mathbf{y}_k$ is only conditionally dependent on the current state $\mathbf{x}_k$, therefore the following relationships can be produced:

$$p(\mathbf{x}_k|\mathbf{x}_{k-1}, ..., \mathbf{x}_0) = p(\mathbf{x}_k|\mathbf{x}_{k-1}) \tag{5.3}$$
$$p(\mathbf{y}_k|\mathbf{x}_k, ..., \mathbf{x}_0) = p(\mathbf{y}_k|\mathbf{x}_k) \tag{5.4}$$

When splitting the observed measurement set into data from the current time instant and data from the previous time instants and using Bayes' law the posterior distribution can be described as

$$p(\mathbf{x}_k|\mathbf{y}_{1:k}) = p(\mathbf{x}_k|\mathbf{y}_k, \mathbf{y}_{1:k-1}) = \frac{p(\mathbf{y}_k|\mathbf{x}_k, \mathbf{y}_{1:k-1})p(\mathbf{x}_k|\mathbf{y}_{1:k-1})}{p(\mathbf{y}_k|\mathbf{y}_{1:k-1})} = \frac{p(\mathbf{y}_k|\mathbf{x}_k)p(\mathbf{x}_k|\mathbf{y}_{1:k-1})}{p(\mathbf{y}_k|\mathbf{y}_{1:k-1})} \tag{5.5}$$

which in turn can be viewed as

$$\text{Posterior} = \frac{\text{Likelihood} \cdot \text{Prior}}{\text{Normalization factor}}. \tag{5.6}$$

The normalization factor ensures that the posterior density integrates to one, therefore if this term is ignored the expression can instead be viewed as

$$\text{Posterior} \propto \text{Likelihood} \cdot \text{Prior}. \tag{5.7}$$

The prior also called the predicted density is described via the Chapman-Kolmogorov equation by marginalizing over the preceding time step according to:

$$p(\mathbf{x}_k|\mathbf{y}_{1:k-1}) = \int p(\mathbf{x}_k|\mathbf{x}_{k-1})p(\mathbf{x}_{k-1}|\mathbf{y}_{1:k-1})\ \mathrm{d}\mathbf{x}_{k-1} \tag{5.8}$$

The distribution, $p(\mathbf{x}_k|\mathbf{x}_{k-1})$ in (5.3) which also occurs in (5.8) are in filtering terms often recognized as the motion model which is used in the prediction step. The second term in (5.8) is the posterior distribution at time $k-1$ which is used in the update step at time $k-1$ and in the prediction step at time k.

The densities in (5.3) and (5.4) are given by a motion model and a measurement model respectively [18, p.20]. These models are generally expressed as:

$$\mathbf{x}_k = f_{k-1}(\mathbf{x}_{k-1}, \mathbf{u}_k) + \mathbf{q}_{k-1} \tag{5.9}$$
$$\mathbf{y}_k = h_k(\mathbf{x}_k, \mathbf{u}_k) + \mathbf{r}_k \tag{5.10}$$

5.2 The Kalman filter

The well known Kalman filter (KF) presented in [19] is a recursive algorithm that uses statistical knowledge and observations of a series of measurements to estimate

unknown parameters. The Kalman filter recursively computes optimal estimates of elements of the Gaussian distribution namely, a mean value and a variance. These elements are represented as a state vector $\hat{\mathbf{x}}_{k|k}$ and a covariance matrix $\mathbf{P}_{k|k}$ at time instant k.

With the assumption that the motion model and the measurement model(s) are linear and with additive Gaussian noise the Kalman filter equations can be derived with its basis on Bayesian filtering presented in Section 5.1, (5.9) and (5.10) to the expressions

$$\mathbf{x}_k = \mathbf{A}_{k-1}\mathbf{x}_{k-1} + \mathbf{B}_{k-1}\mathbf{u}_k + \mathbf{q}_{k-1} \tag{5.11}$$
$$\mathbf{y}_k = \mathbf{H}_k\mathbf{x}_k + \mathbf{B}_k\mathbf{u}_k + \mathbf{r}_k \tag{5.12}$$

where the process and measurement noises are $\mathbf{q}_{k-1} \sim \mathcal{N}(\mathbf{0}, \mathbf{Q_{k-1}})$ and $\mathbf{r}_k \sim \mathcal{N}(\mathbf{0}, \mathbf{R_k})$ respectively.

First the prediction step is derived from (5.8), where $\hat{\mathbf{x}}_{k|k-1}$ is the estimated mean value and $\mathbf{P}_{k|k-1}$ is the estimated covariance matrix. Then the prediction step can be formed as:

$$\hat{\mathbf{x}}_{k|k-1} = \mathbf{A}_{k-1}\hat{\mathbf{x}}_{k-1|k-1} + \mathbf{B}_{k-1}\mathbf{u}_k \tag{5.13}$$
$$\mathbf{P}_{k|k-1} = \mathbf{A}_{k-1}\mathbf{P}_{k-1|k-1}\mathbf{A}_{k-1}^T + \mathbf{Q}_{k-1} \tag{5.14}$$

where $\mathbf{A}_{k-1}$ is the motion model which models the system dynamics and $\mathbf{Q}_{k-1}$ is the process covariance matrix which captures the inaccuracies in the motion model.

Secondly the measurement update step is used to update the mean value $\hat{\mathbf{x}}_{k|k}$ and covariance matrix $\mathbf{P}_{k|k}$ with new observed measurements $\mathbf{y}_k$ from the sensor(s) according to:

$$\mathbf{S}_k = \mathbf{H}_k\mathbf{P}_{k|k-1}\mathbf{H}_k^T + \mathbf{R}_k \tag{5.15}$$
$$\mathbf{K}_k = \mathbf{P}_{k|k-1}\mathbf{H}_k^T\mathbf{S}_k^{-1} \tag{5.16}$$
$$\mathbf{v}_k = \mathbf{y}_k - \mathbf{H}_k\hat{\mathbf{x}}_{k|k-1} \tag{5.17}$$

$$\hat{\mathbf{x}}_{k|k} = \hat{\mathbf{x}}_{k|k-1} + \mathbf{K}_k\mathbf{v}_k \tag{5.18}$$
$$\mathbf{P}_{k|k} = \mathbf{P}_{k|k-1} - \mathbf{K}_k\mathbf{S}_k\mathbf{K}_k^T \tag{5.19}$$

Here the result is a Gaussian posterior density, $\mathcal{N}(\mathbf{x}_k; \hat{\mathbf{x}}_{k|k}, \mathbf{P}_{k|k})$ where the estimated density $\mathbf{x}_k$ has the mean value $\hat{\mathbf{x}}_{k|k}$ and covariance $\mathbf{P}_{k|k}$. These steps in the prediction and measurement update step are iterated for each time instant k to recursively find the posterior density at each time step.

5.3 Sigma point methods

The main idea with sigma point methods is to compute

$$\int f(\mathbf{x})\mathcal{N}(\mathbf{x};\hat{\mathbf{x}},\mathbf{P})\mathrm{d}\mathbf{x} \tag{5.20}$$

to perform Gaussian filtering. However it is often hard to compute this integral and therefore the approximation

$$\int f(\mathbf{x})\mathcal{N}(\mathbf{x};\hat{\mathbf{x}},\mathbf{P})\mathrm{d}\mathbf{x} \approx \sum_{i=1}^{N} w^{(i)} f(\chi^{(i)}) \tag{5.21}$$

is often used instead, where $\chi^{(i)}$ are called σ-points and $w^{(i)}$ are weights.

5.3.1 The Cubature Kalman Filter

In order to compute a Cubature Kalman filter a set of $2n$ σ-points is formed, where n is the dimension of $\mathbf{x}$, i.e. the number of states. The sigma points are then formed according to:

$$\chi_{k-1}^{(i)} = \hat{\mathbf{x}}_{k-1|k-1} + \sqrt{n}\mathbf{P}^{\frac{1}{2}}_{(k-1|k-1)i}, \quad i = 1,..,n \tag{5.22}$$

$$\chi_{k-1}^{(i+n)} = \hat{\mathbf{x}}_{k-1|k-1} - \sqrt{n}\mathbf{P}^{\frac{1}{2}}_{(k-1|k-1)i}, \quad i = 1,..,n \tag{5.23}$$

where $\mathbf{P}_i^{\frac{1}{2}}$ is the i:th column of $\mathbf{P}^{\frac{1}{2}}$ that fulfills $\mathbf{P}^{\frac{1}{2}} \cdot \mathbf{P}^{\frac{1}{2}T} = \mathbf{P}$.

The weights are formed as:

$$w^{(i)} = \frac{1}{2n}, \quad i = 1,..,2n \tag{5.24}$$

When the sigma points and their weights have been calculated the predicted moments are estimated with

$$\hat{\mathbf{x}}_{k|k-1} \approx \sum_{i=1}^{2n} \mathbf{f}(\chi_{k-1}^{(i)}) w^{(i)} \tag{5.25}$$

$$\mathbf{P}_{k|k-1} \approx \mathbf{Q}_{k-1} + \sum_{i=1}^{2n} \left(\mathbf{f}(\chi_{k-1}^{(i)}) - \hat{\mathbf{x}}_{k|k-1}\right)\left(\mathbf{f}(\chi_{k-1}^{(i)}) - \hat{\mathbf{x}}_{k|k-1}\right)^T w^{(i)} \tag{5.26}$$

In the update step a new set of $2n$ σ-points is formed together with the weights:

$$\chi_{k}^{(i)} = \hat{\mathbf{x}}_{k|k-1} + \sqrt{n}\mathbf{P}^{\frac{1}{2}}_{(k|k-1)i}, \quad i = 1,..,n \tag{5.27}$$

$$\chi_{k}^{(i+n)} = \hat{\mathbf{x}}_{k|k-1} - \sqrt{n}\mathbf{P}^{\frac{1}{2}}_{(k|k-1)i}, \quad i = 1,..,n \tag{5.28}$$

$$w^{(i)} = \frac{1}{2n}, \quad i = 1,..,2n \tag{5.29}$$

These new σ-points are used for estimating the desired moments as:

$$\hat{\mathbf{y}}_{k|k-1} \approx \sum_{i=1}^{2n} \mathbf{h}\left(\chi_k^{(i)}\right) w^{(i)} \tag{5.30}$$

$$\mathbf{P}_{xy} \approx \sum_{i=1}^{2n} \left(\chi_k^{(i)} - \hat{\mathbf{x}}_{k|k-1}\right)\left(\mathbf{h}(\chi_k^{(i)}) - \hat{\mathbf{y}}_{k|k-1}\right)^T w^{(i)} \tag{5.31}$$

$$\mathbf{S}_k \approx \mathbf{R}_k + \sum_{i=1}^{2n} \left(\mathbf{h}(\chi_k^{(i)}) - \hat{\mathbf{y}}_{k|k-1}\right)\left(\mathbf{h}(\chi_k^{(i)}) - \hat{\mathbf{y}}_{k|k-1}\right)^T w^{(i)} \tag{5.32}$$

The estimated states and their covariance can then be calculated using the following equations:

$$\hat{\mathbf{x}}_{k|k} = \hat{\mathbf{x}}_{k|k-1} + \mathbf{P}_{xy}\mathbf{S}_k^{-1}(\mathbf{y}_k - \hat{\mathbf{y}}_{k|k-1}) \tag{5.33}$$

$$\mathbf{P}_{k|k} = \mathbf{P}_{k|k-1} - \mathbf{P}_{xy}\mathbf{S}_k^{-1}\mathbf{P}_{xy}^T \tag{5.34}$$

These estimations are then used in the next iteration of the CKF.

5.4 Kalman Filter Implementation

By using a linear motion model a Kalman Filter can be used in order to fuse sensor data. Here a constant velocity model (CV) is used as motion model. By using a CV model some dynamics of the state evolution is created which should result in a better estimation than what is achieved with the current implementation. The choice of CV model is an initial guess to see if the model can capture the NO_x formation behaviour, if instead no motion model is used the filter can be considered to be powered by noise also called random walk which really does not take any system dynamics into consideration. So to be able to catch some system dynamics the CV model was considered to be better to use than a random walk. The CV model uses two states

$$\mathbf{x}_k = \begin{bmatrix} NO_x \\ \frac{dNO_x}{dt} \end{bmatrix}. \tag{5.35}$$

These states are connected by the motion model

$$\mathbf{x}_k = \underbrace{\begin{bmatrix} 1 & T \\ 0 & 1 \end{bmatrix}}_{\mathbf{A}_{k-1}} \mathbf{x}_{k-1} + \mathbf{q}_{k-1} \tag{5.36}$$

where T is the sample time. The process covariance matrix was determined to be

$$\mathbf{Q}_{k-1} = \begin{bmatrix} \frac{T^3}{3} & \frac{T^2}{2} \\ \frac{T^2}{2} & T \end{bmatrix} \cdot \sigma_{cv}^2 \tag{5.37}$$

where $\sigma_{cv} = 1.2$ was found after some tuning based on trial and error.

In order for the filter to be able to use information from the sensors a measurement model is also needed. Since one of the states in $\mathbf{x_k}$ is NO_x and it exists three measured signals that can be compared to the NO_x state then the measurement model is formed as

$$\mathbf{y}_k = \underbrace{\begin{bmatrix} 1 & 0 \\ 1 & 0 \\ 1 & 0 \end{bmatrix}}_{\mathbf{H}_k} \mathbf{x}_k + \mathbf{r}_k. \tag{5.38}$$

The three measurement signals are from one physical sensor and the other two originate from empirically determined models for NO_x formation here seen as virtual sensors.

5.5 Cubature Kalman Filter Implementation

Since engine out NO_x is the state that is to be estimated with the Cubature Kalman filter (CKF), this is then needed to be a part of the state vector. Since the previously developed NO_x model needs certain inputs these are also chosen as states. The state vector does therefore look like

$$\mathbf{x}_k = \begin{bmatrix} NO_x \\ rpm \\ fuelInj \\ \alpha SOI \\ \alpha EOI \\ boostP \end{bmatrix}. \tag{5.39}$$

The models for estimation of cylinder pressure, cylinder temperature and NO_x are combined to create the non linear motion model in the Cubature Kalman filter, $f_{k-1}(\mathbf{x}_{k-1}, \mathbf{u}_k)$. Since all states can be accessed as measurements they are considered as input signals to the motion model with the exception of NO_x which is estimated through the model. The complete motion model does therefore become

$$\begin{bmatrix} NO_x \\ rpm \\ fuelInj \\ \alpha SOI \\ \alpha EOI \\ boostP \end{bmatrix} = \underbrace{\begin{bmatrix} f_{k-1}(\mathbf{x}_{k-1}) \\ 0 \\ 0 \\ 0 \\ 0 \\ 0 \end{bmatrix} + \begin{bmatrix} 0 & 0 & 0 & 0 & 0 \\ 1 & 0 & 0 & 0 & 0 \\ 0 & 1 & 0 & 0 & 0 \\ 0 & 0 & 1 & 0 & 0 \\ 0 & 0 & 0 & 1 & 0 \\ 0 & 0 & 0 & 0 & 1 \end{bmatrix} \begin{bmatrix} rpm \\ fuelInj \\ \alpha SOI \\ \alpha EOI \\ boostP \end{bmatrix}}_{f_{k-1}(\mathbf{x}_{k-1}, \mathbf{u}_k)} + \mathbf{q}_{k-1}. \tag{5.40}$$

The measurements to the CKF are also here seen as three sensors, where one is a physical NO_x sensor and the other two are virtual sensors which in practice are two different empirically determined models for NO_x formation. The output from the developed NO_x model gives the concentration of NO_x as a fraction, which then has to be multiplied with 10^6 in order to get the value in ppm. In order to be able to compare the state with the measurements, the measurement model needs to look like

$$\mathbf{y}_k = \underbrace{\begin{bmatrix} 10^6 & 0 & 0 & 0 & 0 & 0 \\ 10^6 & 0 & 0 & 0 & 0 & 0 \\ 10^6 & 0 & 0 & 0 & 0 & 0 \end{bmatrix}}_{h_k(\mathbf{x}_k, \mathbf{u}_k)} \mathbf{x}_k + \mathbf{r}_k. \tag{5.41}$$

It is clear that the measurement model is linear and can therefore be handled as for a regular Kalman Filter. In order for both the CKF and the KF to work two covariance matrices need to be determined, as described in Section 5.2. The process covariance matrix, $\mathbf{Q_{k-1}}$, is determined by analyzing a set of input data, $\mathbf{u}$, together with measured NO_x and calculating its covariance matrix. This is then used as the process covariance. In order to determine the measurement covariance matrix, $\mathbf{R_k}$, a minimization problem was set up which is further explained in Section 5.6.

As previously mentioned the motion model is non linear and the CKF handles this with the use of sigma points, described in Section 5.3. This method does however create the possibility that the states loose their physical meaning, e.g. if the injected fuel or engine speed become negative which would cause the non linear function to get unstable. Intuitively it would be desirable to restrict the spread of the sigma points in order to get rid of unwanted behaviour. This was done by projecting the infeasible sigma points onto the feasible region, i.e. make sure that the states do not loose their physical meaning and then the filter steps could continue, similar to what is described in [20].

5.6 Measurement covariance matrix determination

The covariance matrices for the two motion models have previously been described in respective implementation sections. In order to determine the measurement covariance matrices for the two filters a minimization problem was set up;

$$\begin{aligned} &\text{minimize} && mse_1 + mse_2 \\ &\text{subject to} && r_1,\ r_2,\ r_3 \geq 0 \end{aligned} \tag{5.42}$$

The objective function was set up in order to minimize the mean squared error of two different data sets, where mse_1 and mse_2 represents the two simulated mean squared errors using the current covariance matrix. The parameters used in order to minimize the objective function are the diagonal elements of the covariance matrix, as can be seen below:

$$R = \begin{bmatrix} r_1 & 0 & 0 \\ 0 & r_2 & 0 \\ 0 & 0 & r_3 \end{bmatrix} \tag{5.43}$$

So for every iteration in the minimization problem a set of parameters, $r_1,\ r_2,\ r_3$, are chosen and the filtering is performed on two different data sets. The mean squared errors are calculated and added together, which is used as the objective function for updating the parameters.

This optimization problem is executed using the `fmincon` function in MATLAB© for both the Kalman filter and the Cubature Kalman filter and therefore yields two different covariance matrices for the two filters.

6
Results

In this chapter the results obtained from the linear Kalman filter and the Cubature Kalman filter based on two different data sets are presented. The two data sets are on purpose chosen to represent two different behaviours, the first set is a set of steady state operating points whereas the second set represents a transient behaviour. The data sets have been collected in an engine test cell which makes it possible to use a larger quantity of sensors and a higher accuracy of the sensors. Since the data was collected in the engine test cell also the engine cell NO_x sensor could be viewed as the ground truth when comparing results. The inputs to the models are however taken from sensors that are available in a commercial vehicle.

6.1 Results from the Kalman Filter

The results presented in this section were obtained from simulations using the Kalman filter with the CV model described in section 5.4. In Figure 6.1 the data set with steady state operating points have been used.

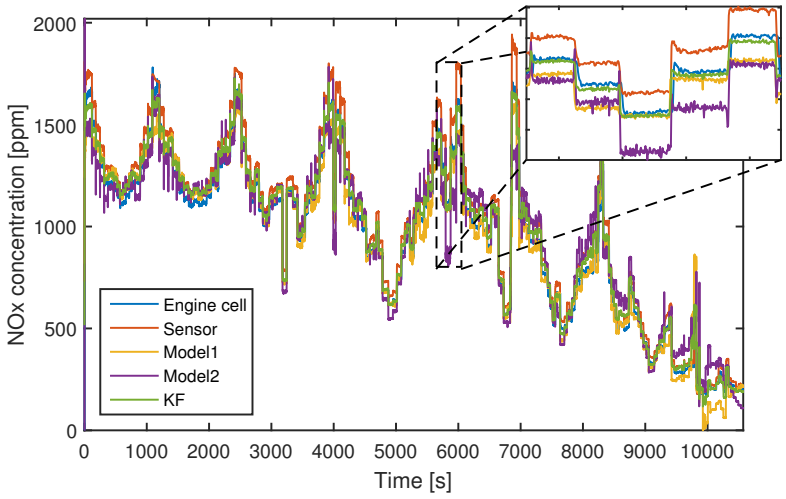

Figure 6.1: *Result from Kalman Filter using a CV-model showing NO_x sensor and model signals together with engine cell NO_x concentration, also a zoomed in section of the result is shown for clarity.*

The illustration shows the engine cell NO_x sensor which is considered as the ground truth, the NO_x sensor, the two empirically determined models and the result from

the Kalman filter. This illustration is included to give an overview of how the different signals behave and it is seen that all the signals seem to have the same trend but differ in magnitude.

In Figure 6.2 the same data set is used but for clarity only the Kalman filtered result together with the engine cell NO_x sensor are shown. As can be seen the Kalman filter follows the desired behaviour relatively correct.

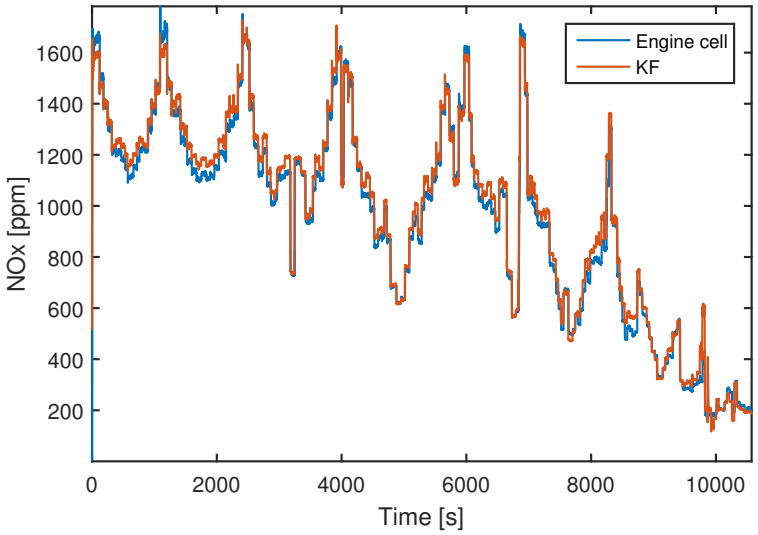

Figure 6.2: *Result from Kalman Filter using a CV-model showing only output from KF and engine cell NO_x concentration.*

In Table 6.1 the mean squared errors are shown for the different models, the NO_x sensor and the Kalman filter result. From this it is evident that the result from the Kalman filter outperforms the other models and the NO_x sensor.

Table 6.1: *Mean squared error for the different models, the NO_x sensor and the Kalman filter for the steady state operating points data set.*

	NO_x sensor	Model1	Model2	KF
MSE ($\cdot 10^3$)	8.89	6.35	10.41	3.53

In Figure 6.3 a zoomed in interval of the result from the transient data set is shown, together with the empirical models and the vehicle sensor.

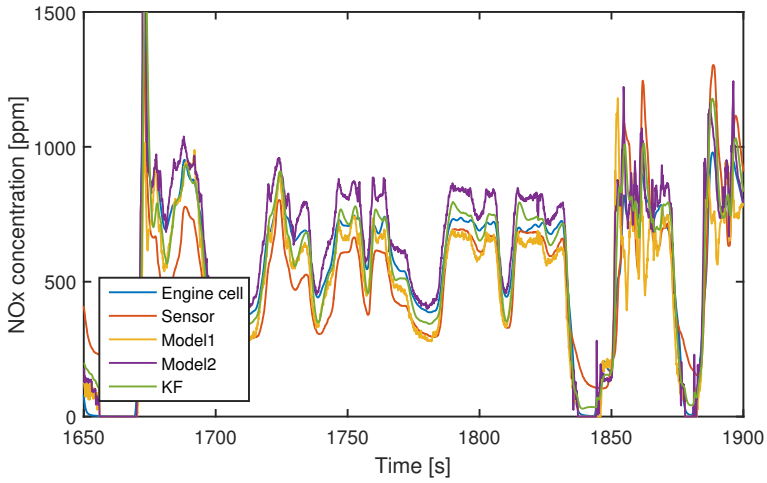

Figure 6.3: *Result from Kalman Filter using a CV-model showing NO_x sensor and model signals together with engine cell NO_x concentration.*

In Figure 6.4 the Kalman filtered result are shown together with the engine cell NO_x sensor for the transient data set. Also for this data set the results from the Kalman filter is satisfactory, in Table 6.2 the mean squared errors for the transient data set are shown. Also in this case the Kalman filter outperforms the other models and the NO_x sensor.

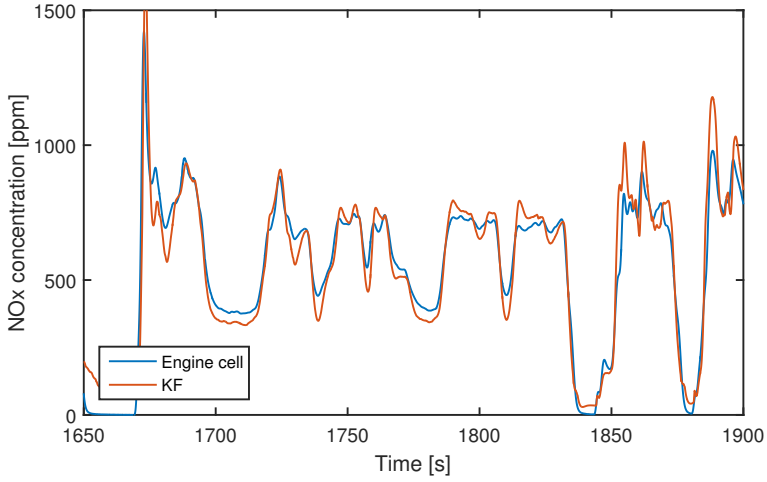

Figure 6.4: *Result from Kalman Filter using a CV-model showing only output from CKF and engine cell NO_x concentration.*

Table 6.2: *Mean squared error for the different models, the NO_x sensor and the Kalman filter for the transient data set.*

	NO_x sensor	Model1	Model2	KF
MSE ($\cdot 10^3$)	24.31	21.25	26.55	6.20

6.2 Results from the Cubature Kalman Filter

The following results were obtained from simulations using the Cubature Kalman filter described in Section 5.5. In Figure 6.5 the different signals and the result from the Cubature Kalman filter for the steady state operating points data set are shown.

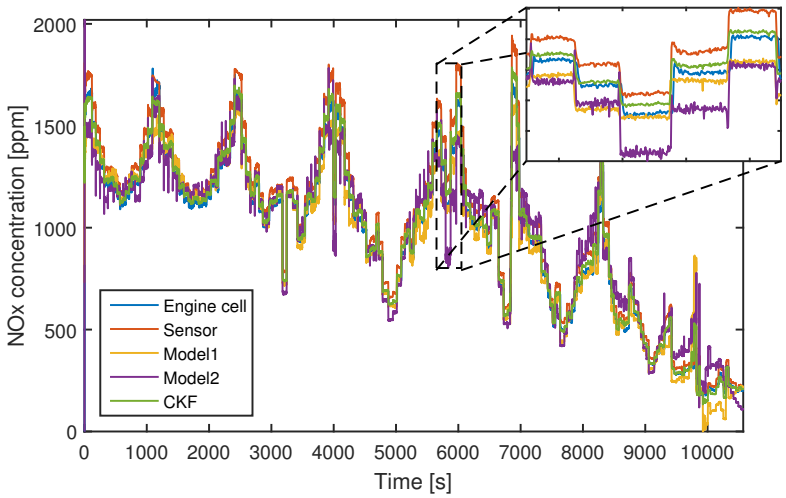

Figure 6.5: *Result from Cubature Kalman Filter showing NO_x sensor and model signals together with engine cell NO_x concentration, also a zoomed in section of the result is shown for clarity.*

In Figure 6.6 only the result from the Cubature Kalman filter and the engine cell NO_x sensor are shown together for clarity using the steady state operating points data set. At a first glance the result looks similar to the result obtained when using the linear Kalman filter, however when the mean squared error is calculated which is shown in Table 6.3 it is clear that the Cubature Kalman filter performs better than the linear Kalman filter.

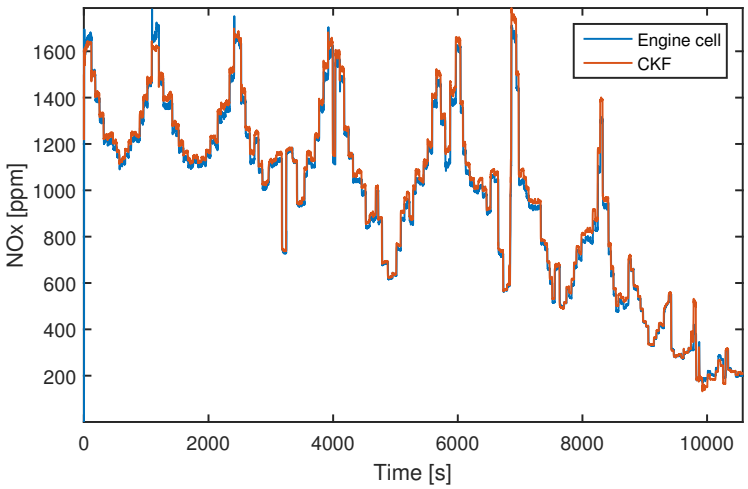

Figure 6.6: *Result from Cubature Kalman Filter showing only output from CKF and engine cell NO_x concentration.*

Table 6.3: *Mean squared error for the different models, the NO_x sensor and the Cubature Kalman filter for the steady state operating points data set.*

	NO_x sensor	Model1	Model2	CKF
MSE $(\cdot 10^3)$	8.89	6.35	10.41	2.73

In Figure 6.7 the result for the Cubature Kalman filter is shown together with the other signals for the transient data set.

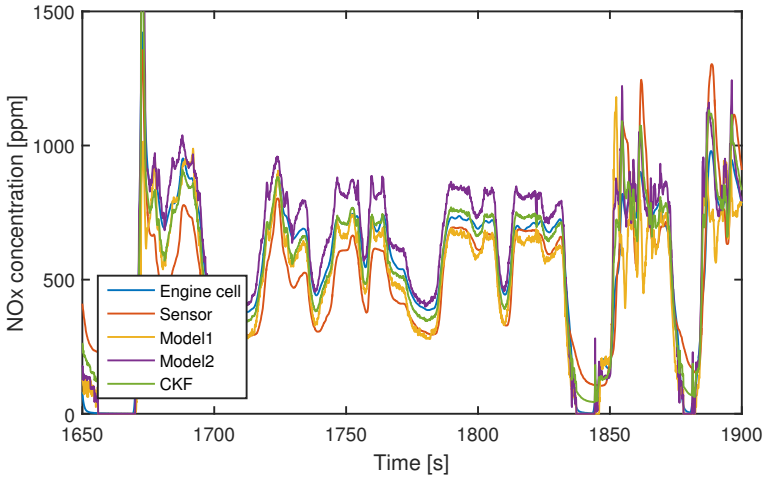

Figure 6.7: *Result from Cubature Kalman Filter showing NO_x sensor and model signals together with engine cell NO_x concentration.*

In Figure 6.8 the result from the Cubature Kalman filter is shown together with the engine cell NO_x sensor. The results obtained from this data set behave in a similar way as the results obtained with the steady state operating points data set.

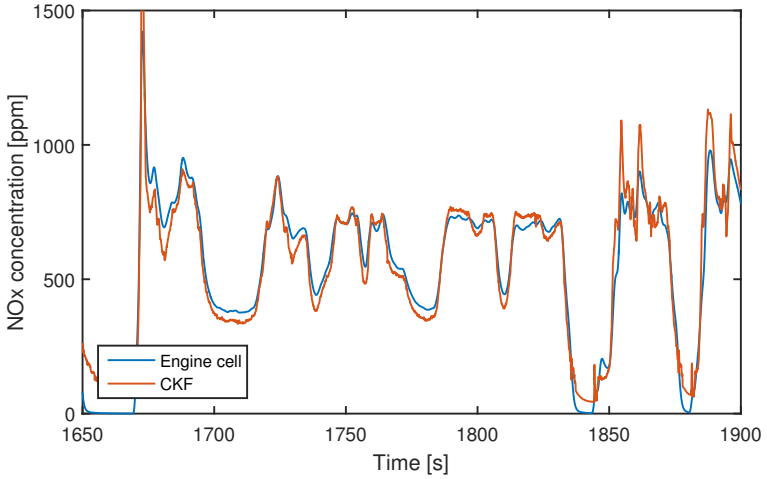

Figure 6.8: *Result from Cubature Kalman Filter showing only output from CKF and engine cell NO_x concentration.*

It is evident from Table 6.4 that also for this data set the Cubature Kalman filter performs better than the NO_x sensor and the two models.

Table 6.4: *Mean squared error for the different models, the NO_x sensor and the Cubature Kalman filter for the transient data set.*

	NO_x sensor	Model1	Model2	CKF
MSE $(\cdot 10^3)$	24.31	21.25	26.55	6.60

6.3 Comparison of Kalman filters

To easier compare the results obtained from the linear Kalman filter and the Cubature Kalman filter a short summary is presented in this section. In Figure 6.9 only the two filtered signals are shown together with the engine cell NO_x sensor signal for the steady state operating points data set.

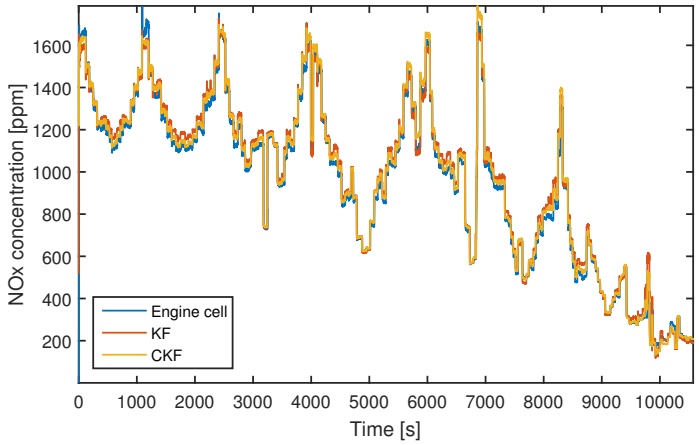

Figure 6.9: *Engine cell NO_x sensor signal, KF signal and CKF signal for steady state operating points data set.*

The two filtered signals are very similar but when calculating the mean squared error it is seen in Table 6.5 that the Cubature Kalman filter performs better.

Table 6.5: *Mean squared error comparison of Kalman filter and Cubature Kalman filter for the steady state operating points data set.*

	KF	CKF
MSE $(\cdot 10^3)$	3.53	2.73

In Figure 6.10 the filtered signals and the engine cell NO_x sensor signal are shown for the transient data set.

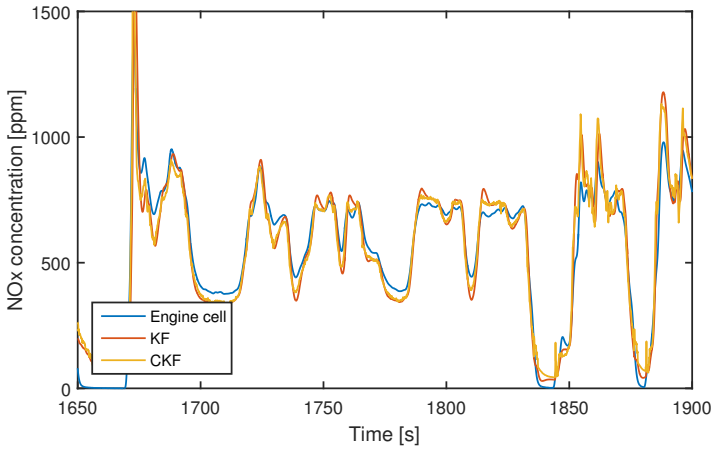

Figure 6.10: *Engine cell NO_x sensor signal, KF signal and CKF signal for transient data set.*

Also for the transient data set the two filtered signals are very similar where only a small variation can be seen in favour of the KF in terms of mean squared error as seen in Table 6.6.

Table 6.6: *Mean squared error comparison of Kalman filter and Cubature Kalman filter for the transient data set.*

	KF	CKF
MSE $(\cdot 10^3)$	6.20	6.60

6.4 Linear regression model

In order to analyze how well the two filters model the NO_x behaviour a linear regression model was created for the two filters; CKF and KF and for the two existing models for the two data sets. The results can be seen in Figure 6.11 for the steady state operating points data set and in Figure 6.12 for the transient data set. A perfect estimation would have the slope 1 and coefficient of determination $R^2 = 1$. This is however not the case but both the CKF and the KF have a higher coefficient of determination than the two existing models for both data sets.

In Figure 6.11 it is seen that the CKF has got a slope that is slightly closer to one than the KF which implies that the estimations from the CKF are more directly related to the measured NO_x than they are for the KF. The CKF also have a slightly higher coefficient of determination.

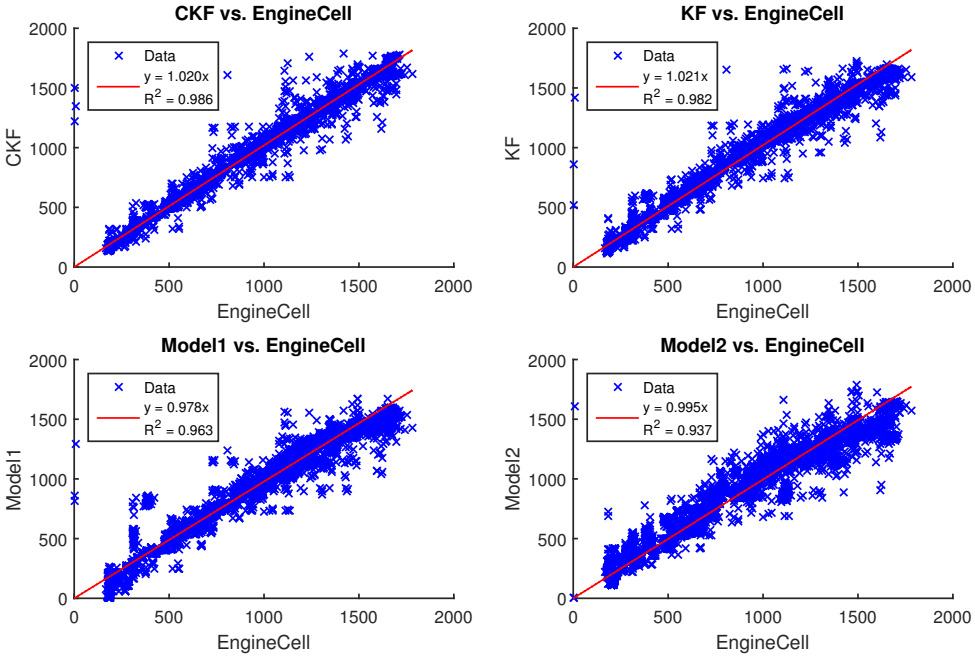

Figure 6.11: *Linear regression model and coefficient of determination for developed filters and existing models, for the steady state operating points data set.*

In Figure 6.12 it can be seen that both the KF and the CKF are very similar, they both have higher coefficient of determination than the two empirical models.

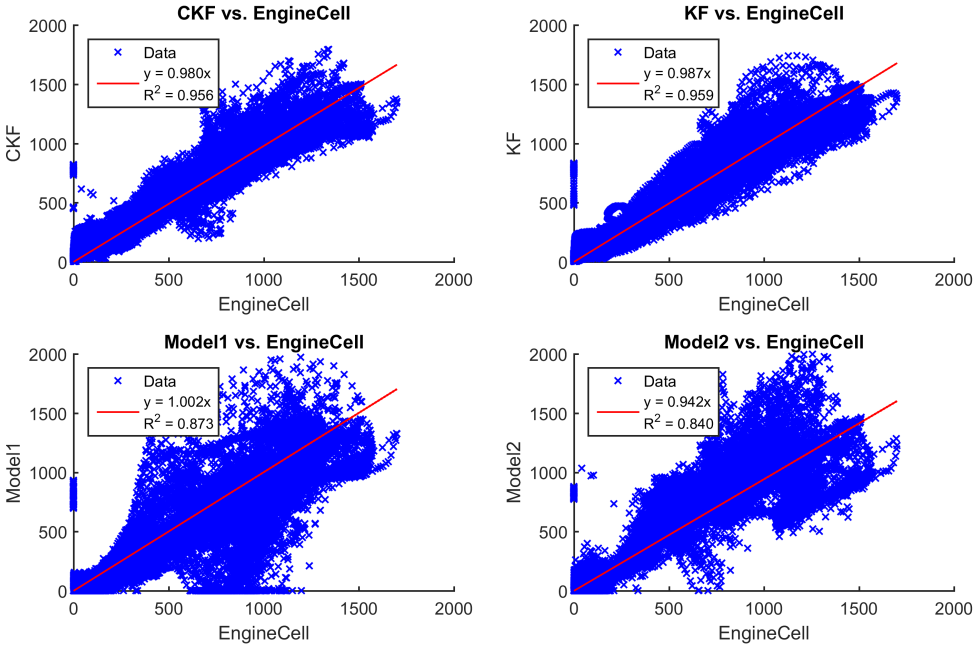

Figure 6.12: *Linear regression model and coefficient of determination for developed filters and existing models, for the transient data set.*

6.5 Simulation time

There is a significant difference in calculation time between the two filters. In Table 6.7 the simulation times can be seen together with how long time it takes for the filter to process one sample. The results are produced using a 2.5GHz laptop using MATLAB© R2015b.

Table 6.7: *Simulation time for the two variations of Kalman filters on the two different sets of data. The simulation time per sample is also shown.*

	Simulation time $[s]$		Time per sample $[s/\text{sample}]$	
	KF	CKF	KF	CKF
Steady state	0.2696	2090	$2.5 \cdot 10^{-5}$	0.1976
Transient	2.3235	18645	$2.2 \cdot 10^{-5}$	0.1743

7
Discussion

There is a trade off between increased accuracy and computation speed. This is evident from the results, the CKF performs better than the KF for the steady state data set in terms of mean squared error. However the KF with the CV model performs similar but is almost 8000 times faster for both the steady state operating points data set as well as for the transient data set. With that in mind it is hard to argue to use the CKF instead of the KF which is way faster and also easier to implement. However when using the CKF the cylinder pressure and cylinder temperature are estimated, so if those variables are of interest for some other function it might be a good idea to use the CKF since other signals that are not available via sensors can be extracted "for free".

As can be seen in the background theory about the *Zeldovich mechanism* in Section 4.1 the model has a large temperature dependence. The cylinder temperature model is the part of this thesis that has proven to be the hardest to validate, due to lack of data to validate against. The effect of this lack of data is that the NO_x estimation become imperfect and does therefore not provide a satisfactory result. An approach that can be used in order to get a better temperature estimation is to reverse engineer the temperature model, such that the final NO_x estimation matches the measured. This approach was however rejected in order to keep the physicality of the temperature model since empirical models are already included in the sensor fusion.

7.1 Different approaches with Kalman filters

As described in Section 5.5 the inputs that are needed for the models are seen as control inputs to the motion model. Another approach was tested where these inputs was seen as measurements instead which led to a more unstable CKF. The instability was due to the fact that when the sigma points where calculated they caused the estimated states to loose their physical meaning, leading to that the models for pressure, temperature and NO_x gave unreliable outputs. This instability was reduced when using the inputs as control inputs with the addition of restricting the sigma points to the feasible region as mentioned in Section 5.5. Similar instability was also experienced when testing yet another way of using the inputs. This approach viewed $fuelInj$, αSOI and αEOI as control inputs, since they can be altered by the engine control. However rpm and $boostP$ was viewed as measurements since these are results of internal processes and cannot be directly controlled

by the engine control unit. These two alternative approaches are represented as state space models and are shown in Appendix A. The choice of filter approach was therefore determined with stability in mind as well as to get a physical meaning of the estimated states as described in Section 5.5.

7.2 Computational efficiency

As seen in Table 6.7 there is a big difference in computational efficiency of the two different Kalman filters. The CKF will not be able to work faster than with a sample time of about 0.2 seconds as it was configured during these simulations. The models for estimating cylinder pressure and temperature are working with a time step of 0.1 CAD, which may not be necessary to obtain a satisfactory result. By using a longer time step for those models the simulation time may be reduced and could be used for a shorter sample time. The difference between the KF and the CKF is however quite large and the KF will always be faster than the CKF.

As seen in Section 4.2 the derived NO_x model constantly underestimates the NO_x concentration, the computational complexity of the model is however assumed to be roughly as high as for a model with a better estimation. The analysis of the difference in computational efficiency are therefore valid even if the NO_x model is updated to perform a better estimation.

The computational efficiency of the KF has not been a subject to optimization in this thesis, it is however possible to create an even faster KF. In Appendix B it can be seen that the Kalman gain rapidly settles to a certain value, which indicates that this gain matrix does not need to be further updated and can therefore be excluded from the update step in order to speed up the filter.

7.3 Future work

Even if the results from this thesis are very promising there are some fields where more work needs to be performed in order to reach an estimator that can be implemented in the engine control strategy. In this section some different subjects that may be interesting to investigate further are discussed.

7.3.1 Possibility of cylinder pressure sensor

In order to reduce the amount of calculations performed by the model a sensor could be used instead of a model that estimates the cylinder pressure. This is nothing that has been used in this thesis and before a possible sensor can be used instead of the model some analysis needs to be performed, as the needed accuracy etc. If the accuracy is good enough a sensor could as mentioned be used in order to speed up the calculations of the NO_x model.

7.3.2 Cylinder temperature model

As seen during this thesis the NO_x model is very sensitive to the cylinder temperature. Since the derived NO_x model does not produce a very precise result, the cylinder temperature model would need more work. The NO_x model was used in this thesis in order to get a better description of how the dynamics of the NO_x formation looks. If the cylinder temperature model would have a better estimation with respect to the cylinder wall temperature, the NO_x model would be even better at describing the dynamics between combustion cycles. As a result from this the NO_x model would likely be even more reliable and the final result would become better as well.

7.3.3 Adaptive covariance matrices

The implemented filters have stationary process/measurement covariance matrices which are responsible for determining how much each sensor or model should influence the estimation. Analysis of the models and sensors have shown that they yield diverse estimations for different phases of the data sets. In order to really answer some of the questions in Section 1.1 a closer analysis of the models and sensors is needed. Such analysis may contribute to a better understanding of when the different models and sensors should influence more or less. This knowledge should influence the covariance matrices and result in an even better estimation by the Kalman filters.

8

Conclusion

The results presented in this report show that using sensor fusion techniques in order to better estimate engine out NO_x is a promising approach. Both of the developed filters yield better estimations in terms of mean squared errors than using either of the existing models or sensors separately. Even though the fact that the derived NO_x model does not give an adequate output in terms of absolute values, the CKF using the derived NO_x model as motion model yields a satisfactory result. Although the linear Kalman filter performs worse than the CKF in steady state it has an extensive advantage in terms of computational efficiency. The KF is also straight forward to implement which is not the case for the CKF. Since the linear Kalman filter with the constant velocity model as motion model is almost 8000 times faster than the CKF on average but at the same time performs just slightly worse than the CKF we would recommend to use the linear Kalman filter in a real world implementation, assuming that the cylinder pressure or cylinder temperature is not of interest for some other process in the ECU.

Future work would need to involve better knowledge about the sensors and the empirically determined models and at what conditions they are reliable or not. Investigations of this would yield chance to adapt the covariance matrices iterative to reach an even better result.

Bibliography

[1] İ. A. Reşitoğlu, K. Altinişik, and A. Keskin, "The pollutant emissions from diesel-engine vehicles and exhaust aftertreatment systems," *Clean Technologies and Environmental Policy*, vol. 17, no. 1, pp. 15–27, 2015. [Online]. Available: http://dx.doi.org/10.1007/s10098-014-0793-9

[2] R. J. Blaszczak, "Nitrogen oxides (nox): Why and how they are controlled," U.S. environmental protection agency, Research Triangle Park, North Carolina, Tech. Rep. EPA-456/F-99-006R, November 1999. [Online]. Available: https://www3.epa.gov/ttncatc1/cica/other7_e.html

[3] G. A. Lavoie, J. B. Heywood, and J. C. Keck, "Experimental and theoretical study of nitric oxide formation in internal combustion engines," *Combustion Science and Technology*, vol. 1, no. 4, pp. 313–326, 1970. [Online]. Available: http://dx.doi.org/10.1080/00102206908952211

[4] A. Kalyan and I. K. Puri, *Combustion Science and Engineering*. Boca Raton, Florida: CRC Press, 2007.

[5] J. E. Dec, "A conceptual model of di diesel combustion based on laser-sheet imaging*," in *SAE Technical Paper*. SAE International, 02 1997. [Online]. Available: http://dx.doi.org/10.4271/970873

[6] EC, "Commission directive 2005/78/ec," *Official Journal of the European Union*, p. 21, November 2005. [Online]. Available: http://eur-lex.europa.eu/legal-content/EN/TXT/PDF/?uri=CELEX:32005L0055&from=EN

[7] EU, "Regulation (ec) 595/2009," *Official Journal of the European Union*, p. 10, July 2009. [Online]. Available: http://eur-lex.europa.eu/legal-content/EN/TXT/PDF/?uri=CELEX:32009R0595&from=EN

[8] C. Guardiola, B. Pla, D. Blanco-Rodriguez, and P. O. Calendini, "Ecu-oriented models for nox prediction. part 1: a mean value engine model for nox prediction," *Proceedings of the Institution of Mechanical Engineers, Part D: Journal of Automobile Engineering*, vol. 229, no. 8, pp. 992–1015, 2015;2014;. [Online]. Available: http://dx.doi.org/10.1177/0954407014550191

[9] R. Stobart and Z. Yang, "A control-oriented nox emissions model for diesel engines," *International Journal of Powertrains*, vol. 5, no. 2, pp. 191–210, 2016. [Online]. Available: http://www.inderscienceonline.com/doi/abs/10.1504/IJPT.2016.076570

[10] R. Miller, G. Davis, G. Lavoie, C. Newman, and T. Gardner, "A super-extended zel'dovich mechanism for nox modeling and engine calibration," in *SAE Technical Paper*. SAE International, 02 1998. [Online]. Available: http://dx.doi.org/10.4271/980781

[11] C. Ericson, B. Westerberg, M. Andersson, and R. Egnell, "Modelling diesel engine combustion and nox formation for model based control and simulation of engine and exhaust aftertreatment systems," in *SAE Technical Paper*. SAE International, 04 2006. [Online]. Available: http://dx.doi.org/10.4271/2006-01-0687

[12] G. Woschni, "A universally applicable equation for the instantaneous heat transfer coefficient in the internal combustion engine," in *SAE Technical Paper*. SAE International, 02 1967. [Online]. Available: http://dx.doi.org/10.4271/670931

[13] R. C. Flagan and J. H. Seinfeld, *Fundamentals of air pollution engineering*. Englewood Cliffs, New Jersey: Prentice-Hall, Inc., 1988. [Online]. Available: http://resolver.caltech.edu/CaltechBOOK:1988.001

[14] M. W. Chase, *NIST-JANAF Thermochemical Tables*. Washington, DC: American Institute of Physics for the National Institute of Standards and Technology, 1998. [Online]. Available: http://kinetics.nist.gov/janaf/

[15] Gamma Technologies. (2016) GT-POWER engine simulation software. [Online]. Available: https://www.gtisoft.com/gt-suite-applications/propulsion-systems/gt-power-engine-simulation-software

[16] J. Heywood, *Internal Combustion Engine Fundamentals*, ser. Automotive technology series. McGraw-Hill, 1988.

[17] S. Särkkä, *Bayesian Filtering and Smoothing*, ser. Institute of Mathematical Statistics Textbooks. Cambridge University Press, 2013.

[18] M. Lundgren, *Bayesian filtering for automotive applications*. Department of Signals and Systems, Signal Processing, Chalmers University of Technology, 2015.

[19] R. E. Kalman, "A new approach to linear filtering and prediction problems," *Transactions of the ASME–Journal of Basic Engineering*, vol. 82, no. Series D, pp. 35–45, 1960. [Online]. Available: https://www.cs.unc.edu/~welch/kalman/media/pdf/Kalman1960.pdf

[20] R. Kandepu, L. Imsland, and B. A. Foss, "Constrained state estimation using the unscented kalman filter," in *2008 16th Mediterranean Conference on Control and Automation*, June 2008, pp. 1453–1458.

A

Alternative filter structures

Cubature Kalman filter where the inputs needed for the developed models are seen as measurements

$$\underbrace{\begin{bmatrix} NO_{\mathrm{x}} \\ rpm \\ fuelInj \\ \alpha SOI \\ \alpha EOI \\ boostP \end{bmatrix}}_{\mathbf{x}_k} = \underbrace{\begin{bmatrix} f_{k-1}(\mathbf{x}_{k-1}) \\ 0 \\ 0 \\ 0 \\ 0 \\ 0 \end{bmatrix}}_{f_{k-1}(\mathbf{x}_{k-1},\mathbf{u}_k)} + \mathbf{q}_{k-1}$$

$$\mathbf{y}_k = \underbrace{\begin{bmatrix} 10^6 & 0 & 0 & 0 & 0 & 0 \\ 10^6 & 0 & 0 & 0 & 0 & 0 \\ 10^6 & 0 & 0 & 0 & 0 & 0 \\ 0 & 1 & 0 & 0 & 0 & 0 \\ 0 & 0 & 1 & 0 & 0 & 0 \\ 0 & 0 & 0 & 1 & 0 & 0 \\ 0 & 0 & 0 & 0 & 1 & 0 \\ 0 & 0 & 0 & 0 & 0 & 1 \end{bmatrix}}_{h_k(\mathbf{x}_k,\mathbf{u}_k)} \mathbf{x}_k + \mathbf{r}_k$$

Cubature Kalman filter where some of the inputs needed for the developed models are seen as control inputs to the motion model and some inputs are seen as measurements.

$$\underbrace{\begin{bmatrix} NO_{\mathrm{x}} \\ rpm \\ fuelInj \\ \alpha SOI \\ \alpha EOI \\ boostP \end{bmatrix}}_{\mathbf{x}_k} = \underbrace{\begin{bmatrix} f_{k-1}(\mathbf{x}_{k-1}) \\ 0 \\ 0 \\ 0 \\ 0 \\ 0 \end{bmatrix} + \begin{bmatrix} 0 & 0 & 0 \\ 0 & 0 & 0 \\ 1 & 0 & 0 \\ 0 & 1 & 0 \\ 0 & 0 & 1 \\ 0 & 0 & 0 \end{bmatrix} \begin{bmatrix} fuelInj \\ \alpha SOI \\ \alpha EOI \end{bmatrix}}_{f_{k-1}(\mathbf{x}_{k-1},\mathbf{u}_k)} + \mathbf{q}_{k-1}$$

$$\mathbf{y}_k = \underbrace{\begin{bmatrix} 10^6 & 0 & 0 & 0 & 0 & 0 \\ 10^6 & 0 & 0 & 0 & 0 & 0 \\ 10^6 & 0 & 0 & 0 & 0 & 0 \\ 0 & 1 & 0 & 0 & 0 & 0 \\ 0 & 0 & 0 & 0 & 0 & 1 \end{bmatrix}}_{h_k(\mathbf{x}_k,\mathbf{u}_k)} \mathbf{x}_k + \mathbf{r}_k$$

B

Kalman gain settling time

The evolution of three elements from the Kalman gain matrix K can be seen below. It is seen that the values settle rapidly to a steady state value.

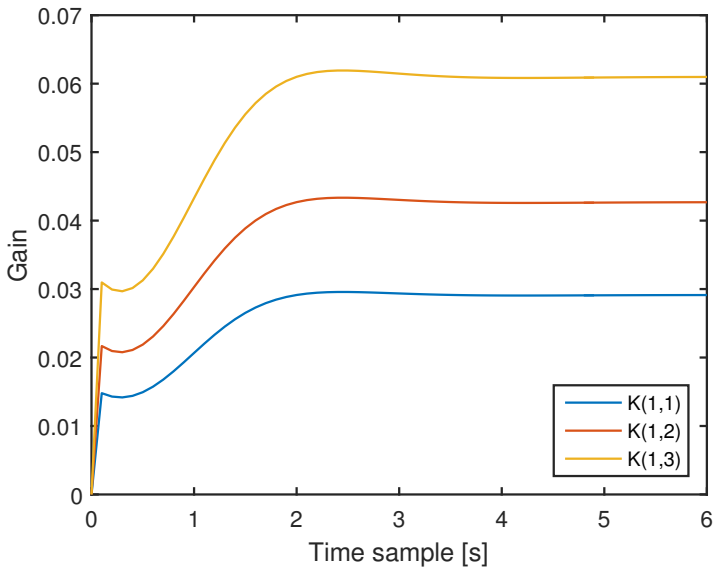

Figure B.1: *Kalman gain settling time for corresponding measurements.*